Evaluation and Repair of Blast Damaged Reinforced Concrete Beams

By

John L. Hudson

David Darwin

A Report on Research Sponsored by

The University of Kansas
Structural Engineering and Materials
Laboratory

Structural Engineering and Engineering Materials
SL Report 05-1

UNIVERSITY OF KANSAS CENTER FOR RESEARCH, INC.
LAWRENCE, KANSAS
January 2005

Abstract

Ten reinforced concrete beams were constructed using standard concrete and A 615 Grade 60 reinforcing steel. Eight of the beams were then damaged using C-4 Composite high explosives to replicate the actual damage that a structural element may receive from a small bomb or other explosive device. The damaged beams were then evaluated and four of the beams were determined to have been damaged beyond reasonable repair. Of the other four damaged beams, two were repaired using carbon fiber reinforced polymer (FRP). The two repaired beams, two unrepaired beams, and two control beams were then tested in third-point loading to determine flexural strength capacity.

The load-deflection curves for the six beams were then analyzed to evaluate the effect of the FRP repairs. The two repaired beams demonstrated significant improvement in flexural strength over the unrepaired beams and equaled or exceeded the flexural strength of the undamaged control beams.

The study demonstrated that fiber reinforced polymers represent a viable option for the repair of blast damaged beams. The FRP repaired beams demonstrated a significant improvement in flexural capacity in comparison to their equivalently damaged counterparts.

Keywords: blast load, reinforced concrete beam, FRP repair

Acknowledgements

This report was prepared by MAJ John Hudson in partial fulfillment of the requirements of the MSCE degree from the University of Kansas. The research was supported by the Structural Engineering and Materials Laboratory at the University of Kansas. I would like to thank a number of individuals for there support and contributions during this project. The project advisor was Dr. David Darwin, Professor of Civil, Environmental and Architectural Engineering Department at the University of Kansas. LTC Tony Wright and the 70th Engineer Battalion, Fort Riley, Kansas, provided support and resources during the demolition operations. Mr. Will Gold, Composite Engineering Specialist with Watson Bowman Acme Corp, supplied technical advice, as well as all required MBrace© Composite Strengthening System materials. Additionally, Mr. Jim Weaver and Mr. Jay Barnard's efforts in the Structures Testing Laboratories throughout the construction, repair, and testing process were critical to the success of the project.

Table of Contents

Chapter 1

Introduction

1.1 Background

The US Army Corps of Engineers is currently heavily engaged in reconstruction operations in Iraq, including repairing, replacing and upgrading the nation's infrastructure. As a result of both combat operations and terrorism, many structures have endured various levels of blast damage, ranging from complete destruction to superficial scarring of the facades and broken windows. One of the tasks that engineers on the ground face is determining what structures are still safe for use and what structures must be torn down or repaired. Most structures in Iraq are masonry and/or reinforced concrete.

Fiber reinforced polymer (FRP) composite materials are currently being used across the United States in the rehabilitation and repair of our aging infrastructure. FRP is an attractive material for rehabilitation and strengthening of reinforced concrete structures. It provides a high strength-to-weight ratio, is resistance to corrosion, is very durable, simple to install, and has very low maintenance requirements (Kachlakev, Green, and Barnes 2000). As a result, FRP represents a realistic option for the repair and rehabilitation of blast damaged structures.

Currently, the author is unaware of any past or present research on the specific use of FRP to repair blast damaged reinforced concrete structures. There are, however, a number of research projects that have been conducted analyzing the ability of FRP to improve a structure's capability to withstand a blast. In particular, research at the University of Missouri at Rolla has been conducted to evaluate FRP's ability to mitigate the hazards posed by masonry walls under blast loads (Nanni and Gold 1998).

1.2 Problem Statement

The purpose of this study is to evaluate the use of FRP in the repair of reinforced concrete beams that have been damaged by a high explosive blast. Each beam will be evaluated to determine the extent of damage caused by the explosive charge and whether or not repair using FRP, in conjunction with high strength mortar, is a viable option.

1.3 Scope of Project

Four pairs of reinforced concrete beams were blast damaged using Composition C-4 high explosives to replicate actual damage caused to concrete structures by blasts. The blast loads on the beams were adjusted to cause a different level of damage for each set of beams. The damage to the beams was evaluated using visual inspection. Blast force data acquisition was beyond the scope and budget of this project since the primary focus was on the repair of a beam after it was already damaged. Undamaged control beams were tested to determine the relationship between visual cues and remaining strength. One beam from each set of beams that were determined to have sufficient strength to justify repair was repaired using FRP and rapid strength repair mortar. The repaired beams were then tested to determine their load-deflection behavior and failure mode. Their strength was then compared with that of the unrepaired beam from each set and the undamaged control beams.

1.4 Factors Affecting Blast Damage in Structures

There are three primary factors that affect the extent of damage created by a blast (TM 5-855-1 1986).

1. Blast Loading – the force that impacts the structure, as a function of the type, weight, and location of the explosive relative to the structure.
2. Structural Characteristics – the type of structural system used, particularly the external walls and roof.
3. Construction Materials – the type of materials, design details, and quality of construction.

There are two basic categories of structural damage, "local" and "global." Local damage occurs to elements or parts of elements in the structural system. It is usually caused by projectile impact or close proximity detonations of high explosive charges too small to destroy the entire structure. Global damage occurs from high explosive charges large enough to create extensive damage involving several structural members. It can also occur when the loss of an element due to local damage causes progressive collapse of the structure or part of the structure. Progressive collapse results from the inability of the structure to bridge over a local failure (Hamad 1993). For this project, it is assumed that the damage to the beams represents local damage within a structure.

There are three ways that an explosive energy release can impact the structural integrity of a building or structural member:

1. The shock wave - resulting overpressure and underpressure from the blast transmitted through the air.
2. Earth shock wave – it usually has little effect on structures, unless the blast is extremely large, due to the rapid decrease in force that results from energy absorbed by the ground (Walley 1994).
3. Impact of projectiles placed in motion by the blast.

The blast loading in this project was designed so that only the shock wave had a significant effect on the beams.

1.5 Dynamics Behind an Explosion

An explosion is an intense release of energy caused by the violent oxidation of material. The oxidation occurs within just a few milliseconds, depending on the specific kind of explosive used, and produces a highly pressurized volume of very hot gasses. These gasses expand outward at a high rate of speed [Composition C-4 expands at 26,400 ft/s (8050 m/s)]. The expansion exceeds the speed at which air molecules normally respond, resulting in a blast wave. The blast wave is compressed air resulting in an instantaneous rise in pressure (overpressure). The blast wave moves so fast that it overshoots the ambient pressure, resulting in the creation of a vacuum behind the blast wave known as the negative phase (underpressure) (Barakat and Hetherington 1999). The underpressure causes a high air draft to occur, moving from the outer portions of the blast wave back towards the point of detonation. The speed of the blast wave is at first equal to the speed of the detonation [26,400 ft/sec (8050 m/s) for C-4], but then decreases as it propagates spherically away from the point of detonation. The change in pressure caused by the blast wave is illustrated in Figure 1.1.

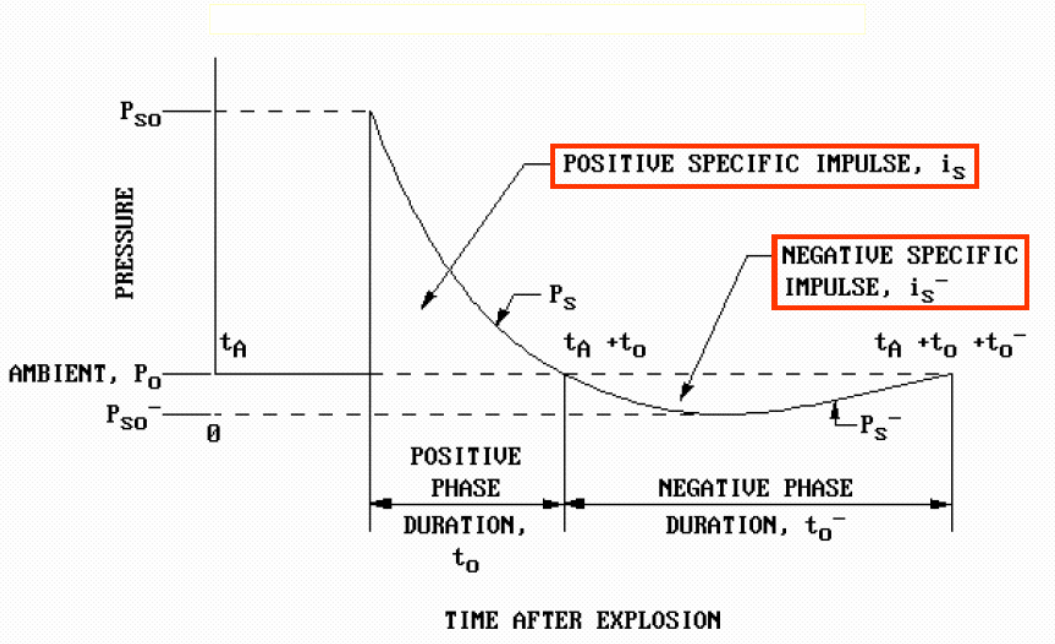

Figure 1.1 Free-field pressure-time variation (TM 5-85-1 1986)

The blast wave produces a pressure force around the structure resulting in the nearly instantaneous overpressure over the entire structure followed by a decrease toward zero overpressure as the blast wave passes (Cabridenc and Garnero 1992). The extent of the deformation of the structure depends on a number of factors, including the type, amount, and distance of the explosive from structure, the shape of the structure, and the structure's ability to absorb the force.

1.6 Location of Blast Detonation

Blast effects are magnified when explosives are detonated within an enclosed space. An excellent example of this is the 1993 bombing at the World Trade Center. A van loaded with explosives was detonated inside the underground parking garage next to the south wall of Tower I. The blast destroyed a large portion of the garage under the Vista Hotel and sent approximately 5000 tons (4,540 Mg) of debris crashing down

through four floors of the parking deck. The debris crushed the heating and refrigeration plant of the World Trade Center complex, which was located 5 stories below ground beneath the underground parking levels (Ramabhushanam and Lynch 1994). The damaged structure consisted primarily of reinforced concrete slabs on steel columns. All of the blast energy was dissipated within the structure, creating enormous impact and reverse loading conditions on the structure, far beyond its design capacity. Reverse loading occurs when structural elements are loaded in the opposite direction of their intended design load, i.e., a beam goes from resisting a gravity load to resisting an uplift force. The slabs failed in shear, creating a crater more than 130 ft (40 m) in diameter and 5 stories deep.

Even relatively small bombs [under 40 lbs (18 kg)] can have a significant impact within a closed space, causing failure of supports and connections. These failures are primarily due to reverse loading of the members resulting in both shear and bending failures.

1.7 Blast Testing

Testing of reinforced concrete members under blast conditions is challenging due to the variability of the blast effects. In addition, the tests are expensive and can be dangerous. To overcome these challenges, blast effects are often simulated through impact tests. The impact tests are more controllable, reproducible, and usually less expensive than explosive tests. Precision impact testing can be used to produce peak loads, rise times, durations, and spatial distributions similar to those produced by explosions (Krauthammer and Zineddin 1999).

Extensive work is being conducted to develop accurate computer modeling of blast and impact effects on both individual structural members and complete structural systems. CONWEP software, developed by the US Army Corps of Engineers and based on Army TM 5-855-1 (1986) was used to model anticipated blast loads on the beams for the different explosive charge weights. This software package is available through the US Army Corps of Engineers - Engineer Research and Development Lab in Vicksburg Mississippi on a controlled distribution basis for official use only.

For this project, blast damage was obtained using Composition C-4 high explosive, not simulated using high impact testing. As a result, differences in the response of the beams varied significantly due to several factors, including the weight of explosives used, firmness of ground beneath the explosive charge, and how well the explosives were packed during the charge assembly. The blast damage portion of the study was incorporated into the demolitions training of the 70th Engineer Battalion at Fort Riley, Kansas. The explosives and associated equipment were provided by the battalion as part of a training exercise in preparation for deployment to Iraq in support of Operation Iraqi Freedom. The University of Kansas Department of Civil, Environmental, and Architectural Engineering provided an additional four reinforced concrete beams and six steel beams for the battalion's use in the demolitions training.

1.8 Rate of Loading Effect

Krauthammer and Zineddin (1999) conducted impact load tests on concrete slabs. These tests demonstrated that reinforced concrete slabs designed to fail in a ductile manner at slow loading rates can fail in a brittle manner under localized impact loads. At

high rates of loading, slabs can fail due to punching shear, with shear cracks appearing in the slab before any significant bending cracks develop. The higher the loading rate, the greater the degree of localized damage or shear failure. Similar behavior can also be seen in the performance of reinforced beams.

1.9 Elastic-Plastic Behavior

Blast pressure can cause significant plastic deformation and large deflections in reinforced concrete members, leading to uniaxial tensile failures or loss of integrity at the supports. Large concentrated impact loads and distributed impulsive loading causes large localized plastic strains, which dominate elastic effects and quickly promote failure by shearing or tearing (Schleyer and Hsu 2000). Even if no visible damage, such as excessive deflection, cracking, or spalling is observed on an individual member, there may still be very fine cracks in the concrete element sufficient to require repair to restore its full strength.

1.10 Analysis of Structures Under Blast Loads

Blast loads are typically analyzed using a single-degree-of-freedom (SDOF) system because they are nonoscillatory loads and only the peak response is required. An SDOF system consists of a mass, a damper, and a spring or resistance element. The mass and spring is selected so that the frequency of the SDOF system will equal the expected response frequency of the actual structure. Because blast loads are nonoscillatory, structural damping can normally be ignored. This enables the use of the following base equation (TM 5-855-1 1986):

$$F(t) - R_R - (M_s\, a) = 0 \qquad (1.1)$$

Where $F(t)$ = forcing function (function of time t)

R_R = resistance function

M_s = mass

a = acceleration

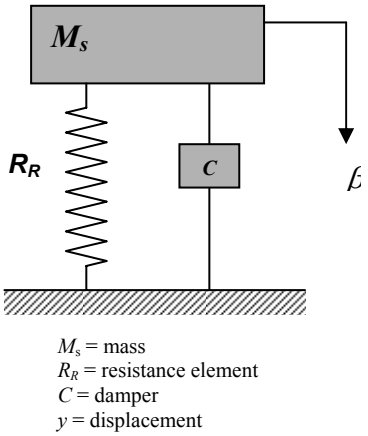

Fig. 1.2 – Single degree of freedom system

1.11 Evaluation of Blast Damage

In practice, a blast damaged structure must first undergo a preliminary investigation to determine the nature and general degree of damage and to ensure that it is stable and safe from progressive structural collapse. This may require taking emergency or temporary protective measures to stabilize the structure. A detailed structural investigation is then conducted, much like one performed for an earthquake-damaged structure. The structural damage is classified in three categories (Hamad 1993):

- Minor damage: Slight cracking, with no observable permanent deformations in the structural element.
- Intermediate damage: Significant cracking, with observable permanent deformations.
- Major damage: Extensive cracking, with gross permanent local or overall deformations.

The structure as a whole is evaluated to determine its strength and stiffness, including the remaining load paths, to explain why certain members sustained damage

and others did not, and to develop repair (or demolition) plans. In-situ nondestructive tests can be conducted as part of the evaluation process. Concrete core samples and reinforcement samples may also be taken for laboratory evaluation.

1.12 Fiber Reinforced Polymer

FRP has a number of advantages over other strengthening systems. These advantages include, high strength and stiffness ratios relative to weight, excellent durability, corrosive resistance, rapid installation, architectural flexibility (easily concealed), and high formability around complex shapes.

1.12.1 Flexural Strengthening using FRP

For flexural strengthening, FRP is usually applied to the surface of the member that is subjected to maximum tension. In the case of a simply supported beam, FRP is applied to the bottom of the beam to increase its flexural strength. The carbon fibers are oriented parallel to the structural member's primary axis. The strength of the member is with FRP in tension is generally controlled by either failure of the concrete in compression or failure of the FRP by tensile fracture (MBrace 2002). The MBrace Engineering Design Guide (MBrace 2002) identifies four failure modes that can occur for a properly applied FRP strengthened system.

- Concrete crushing before steel yielding
- FRP rupture before steel yielding
- Steel yielding followed by concrete crushing
- Steel yielding followed by FRP rupture

The addition of FRP tensile reinforcement can result an overreinforced section with reduced ductility. This can then result in brittle failure because the steel may not yield prior to the crushing of concrete or the rupture of the FRP.

1.12.2 Shear Strengthening using FRP

FRP can be used to increase the shear capacity of a reinforced concrete member by partial or complete beam wrapping (MBrace 2002). There are three primary ways in which FRP can be configured to provide shear reinforcement. The concrete member can be completely wrapped, which provides the maximum shear reinforcement. The member can have the FRP bonded on both sides, which provides the least shear reinforcement. Or the member can be reinforced with a continuous sheet of carbon fiber that wraps from one side to the other across the bottom of the beam, commonly referred to as "U wrapping." For this project, the second layer of carbon fiber (the first layer being the flexural reinforcement) was oriented perpendicular to the beam's primary axis and partially wrapped around the beam in a U-wrap. This method was selected because it is the most commonly used in cases where there is an existing floor slab that prevents full wrapping of the beam.

The MBrace Engineering Design Guide (MBrace 2002) identifies three failure modes that can occur in a properly applied FRP strengthened system loaded in shear.

- Rupture of the FRP sheet
- Debonding of the FRP sheet from the concrete surface
- Significant decrease in the post-cracking concrete shear strength due to a loss of aggregate interlock.

Chapter 2

Experimental Program

2.1 Beam Design and Construction

A total of 14 identical beams were fabricated (10 for this project and four for demolition training by the 70th Engineer Battalion). Each beam was 7 in. (178 mm) wide, 11 in. (280 mm) deep, and 7 ft – 4 in. (2.23 m) long. The longitudinal and transverse reinforcement was the same in all beams.

2.1.1 Size Considerations

The beam sizing was based on selecting the smallest, reasonably sized reinforced beam with the longest span that could be built given the available materials and resources. The results in these tests cannot be extrapolated to larger size beams with any degree of certainty for a variety of reasons, including surface area exposure and distribution of the blast forces, beam proportions, physical characteristics of concrete, and physical characteristics of blast test.

2.1.2 Design Calculations

The beam was sized with the following objectives, limitations, and assumptions:

- Final weight will not exceed 600 lb (270 kg) – a 6 person lift

- Design will be based on ACI 318 (ACI Committee 318 2002) design requirements
- Each form will be able to be constructed from a single sheet of 4 x 8 ft (1.22 x 2.44 m) plywood
- Length will be maximized given the other criteria
- Minimum stirrup spacing is 5 in. (127 mm) based on what can be reasonably constructed given available equipment.
- Tension reinforcement will consist of two reinforcing bars
- All reinforcement will consist of standard size A 615 Grade 60 reinforcing bars
- Concrete strength will be 3500 psi (24 MPa)
- The beam will have a rectangular cross-section and be simply supported at each end
- Compression reinforcement will be used for fabrication to anchor the stirrups, as required by ACI 318-02.

Several cross sections were evaluated where the height of the beam, the depth of the reinforcement, the size of reinforcement, and the length of the stirrups were adjusted. It was determined that using No. 5 (No. 16) bars for the tension reinforcement and No. 3 (No. 10) bars for the compression reinforcement and stirrups provided the optimal beam size of 7 x 11 in. by 7 ft - 4 in. (178 x 280 mm by 2.23 m). The beam cross section is shown in Figure 2.1. Twenty two stirrups were spaced at 4 in. (100 mm) along the beam. The first and the last stirrups were centered 2 in. (50

mm) from the ends of the beam. Based on these bar sizes and beam dimensions, the moment capacity of the beam was determined as follows:

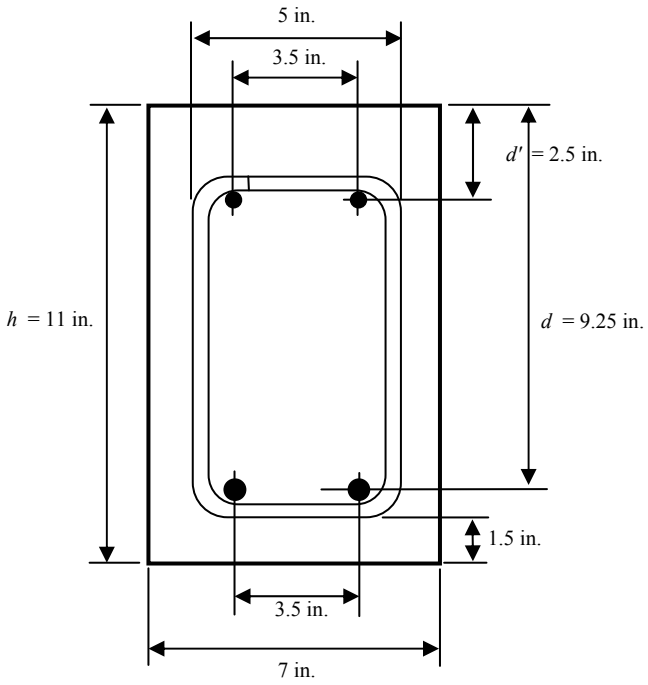

$A_s = 0.62\ \text{in}^2\ (400\ \text{mm}^2)$
$A_s^{'} = 0.22\ \text{in}^2\ (142\ \text{mm}^2)$
$f_y = 60{,}000$ psi (420 MPa)
$f_c^{'} = 3{,}500$ psi (24 MPa)
$l_1 = 6.5$ ft (1.98 m) (distance between anchor points for blast loading)
$l_2 = 6$ ft (1.83 m) (distance between supports for load test)

Fig 2.1 Beam Cross Section

To calculate *a* (distance from extreme compression fiber to centroid of concrete compression) of concrete stress block, an iterative process used Eqs. (2.1) and (2.2) to determine *c* (distance from extreme compression fiber to neutral axis) and f_s (stress in top reinforcement).

$$A_s f_y = A_s^{'} f_s^{'} + 0.85 f_c^{'} \beta_1 c b \qquad (2.1)$$

$$f_s^{'} = \frac{\varepsilon_c (d' - c)}{c E_c} \qquad (2.2)$$

$$a = \beta_1 c \qquad (2.3)$$

Where $\beta_1 = 0.79$

$\varepsilon_c = 0.003$

The concrete compression force at flexural failure is

$$C_c = 0.85 f_c^{'} ba \qquad (2.4)$$

The nominal moment capacity M_n was calculated using Eq. (2.5). Note that the top reinforcement is actually in tension because $C < d$; so the nominal moment capacity is

$$M_n = A_s f_y \left(d - \frac{a}{2} \right) + A_s^{'} f_s^{'} \left(d' - \frac{a}{2} \right) \qquad (2.5)$$

The maximum total load P for the four point bending test is

$$P = \frac{M_n}{l_2 / 3}(2) \qquad (2.6)$$

Based on these equations, the following beam design properties were determined (Table 2.1). The actual material properties were determined through testing, as will be discussed in Sections 2.2.1 and 2.2.2.

Table 2.1 – Beam Section Properties

Material Properties Used in Calculation	f'_c psi (MPa)	f_y psi (MPa)	β_1	c in. (mm)	M_n ft-kips (kN-m)	**Predicted maximum total load** lbs (kN)
Design Properties	3500 (24)	60000 (414)	0.85	2.26 (57.4)	26.4 (35.9)	26400 (117.4)
Actual Material Properties	5160 (35.6)	82000 (565.4)	0.79	2.23 (56.6)	36.4 (49.4)	36400 (161.9)

2.1.3 Construction Process

For beam construction, all component parts were fabricated first. A wood jig was made to ensure proper spacing of the stirrups at 4 in. (100 mm) on center during the reinforcing bar cage assembly (Fig. A.1). All four corners of the stirrups were attached to the longitudinal reinforcement using standard 5 in. (125 mm) wire ties (Fig. A.2). Three reinforcing bar lifting loops were wired to the reinforcing bar cage to facilitate lifting of the beams during testing. The plywood forms (Fig. A.3 and A.4) were constructed using 5/8 in. (16 mm) CDX plywood and 2x4 in. (50 x 100 mm) studs. The forms were treated with form oil prior to placing the reinforcement in the forms to ensure that the form oil did not come in contact with the reinforcement. The reinforcement cage was then placed in the forms supported on two 1½ in. (38 mm) chairs, and anchored to the form using 12 tie wires, six per side. The tie wires were attached to the longitudinal reinforcement and pulled through small holes in the form and secured to the exterior wales.

2.1.4 Casting and Curing

All fourteen beams were cast at the same time from the same batch of ready-mix concrete to minimize variations in material properties for the beams. The concrete was placed in the forms using a concrete bucket with a chute and consolidated by vibration. The forms were removed approximately 72 hours after casting. The beams were covered with burlap and plastic and cured for another five days (Fig. A.5). Eighteen cylinders were cast; six were cured in the curing room, and

twelve were cured adjacent to the beams. After curing, the beams were stored outside, where they were exposed to the elements, including direct sun and rain. Exterior temperatures ranged from the mid 90s to the low 30s. The beams were outside from mid-August until early November.

2.2 Materials

2.2.1 Concrete

Concrete for the fourteen beams was obtained from LRM Inc., a ready mix supplier in Lawrence, Kansas. All fourteen specimens were cast from the same batch of concrete. The concrete used ½ in. (12.5 mm) maximum size limestone. The concrete properties are summarized in Tables 2.1 and 2.2.

Table 2.1 – Concrete Mix Proportions

Material	Proportions
Type I portland cement	470 lb/yd^3 (279 kg/m^3)
Water	197 lb/yd^3 (117 kg/m^3)
Sand	1733 lb/yd^3 (1028 kg/m^3)
Class 1, ½ in (13 mm) diameter max size limestone aggregate	1692 lb/yd^3 (1004 kg/m^3)
Air entraining agent	0.94 oz/yd^3 (35 g/m^3)

Table 2.2 – Concrete Mix Properties

Properties	
Water/Cement Ratio	0.42
Target Strength	3500 psi (24 MPa)
Unit Weight	145.7 lb/ft^3 (2334 kg/m^3)
Slump	2¼ in. (57 mm)
Air Content	3 %

The compressive strength of the concrete was measured using 6 x 12 in. (150 x 300 mm) cylinders. The tests were conducted in accordance with ASTM C 39. Three specimens from the curing room were tested at 28 days. Three of the specimens that had cured along side the beams were tested the day after the beams

Table 2.3 – Compressive Strength of 6 x 12 in. (150 x 300 mm) Cylindrical Concrete Specimens

Specimens	**Individual Cylinder Strength psi (MPa)**	**Average Cylinder Strength psi (MPa)**
28 day wet cured (13 Sep 04)	4260 (29.4)	4260 (29.4)
	4230 (29.2)	
	4300 (29.6)	
Cured along side beams (6 Oct 04 – day after demo range)	4850 (33.4)	4770 (32.9)
	4840 (33.4)	
	4620 (31.9)	
Wet cured (9 Dec 04 - day of flexural loading)	4650 (32.1)	4740 (32.7)
	4760 (32.8)	
	4800 (33.1)	
Cured adjacent to beams (9 Dec 04 - day of flexural loading)	5110 (35.2)	5160 (35.6)
	5220 (36.0)	
	5130 (35.4)	
Wet cured high strength repair mortar (9 Dec 04)	8710 (60.0)	8900 (61.4)
	8690 (59.9)	
	9290 (64.1)	

were damaged at the demolition range to determine the concrete compressive strength in the beams at the time of blast.

A splitting tensile test was conducted on three samples on the same day that the FRP repaired beams were tested to failure (Table 2.4). The test was conducted in accordance with ASTM C 496. All three cylinders were cured adjacent to the beams.

Table 2.4 – Splitting Tensile Strength of 6 x 12 in. (150 x 300 mm) Cylindrical Concrete Specimens

Sample	Average Diameter in. (mm)	Average Length in. (mm)	Maximum Load kip (kN)	Splitting Tensile Strength psi (MPa)
T-1	6.02 (152.9)	12.08 (306.8)	47.5 (211.3)	415 (2.86)
T-2	6.02 (152.9)	12.08 (306.8)	50.5 (224.6)	440 (3.03)
T-3	6.03 (153.1)	12.04 (305.8)	55.0 (244.6)	480 (3.31)

2.2.2 Reinforcement

The reinforcement cages were fabricated using ASTM A 615 grade 60 steel. The longitudinal reinforcement consisted of two No. 5 (No. 16) bars for the tensile reinforcement and two No. 3 (No. 10) bars at the top of the stirrups. Twenty-two No. 3 bar stirrups were used in each beam. Three samples of each size bar were tested. Both bar sizes were tested on an Instron Hydraulic Test Machine under stroke control. The test results are summarized in Table 2.5 and the stress vs. strain curves are shown in Figures 2.1 and 2.2.

Table 2.5 – Reinforcing Bar Properties

Reinforcing Bar Size No.	Sample Number	Yield Strength ksi (MPa)	Tensile Strength ksi (MPa)	Elongation %	Average Yield Strength by Bar Size ksi (MPa)	Average Tensile Strength by Bar Size ksi (MPa)
5 (16)	5-1	84 (579)	100 (689)	12.5	82 (716)	102 (703)
5 (16)	5-2	81 (558)	103 (710)	12.5		
5 (16)	5-3	81 (558)	103 (710)	15.6		
3 (10)	3-1	66 (455)	106 (731)	19.8	66 (455)	104 (717)
3 (10)	3-2	66 (455)	103 (710)	17.2		
3 (10)	3-3	65 (448)	103 (710)	15.6		

All of the No. 5 (No. 16) bars were from the same heat of steel, as were the No. 3 (No. 10) bars. Test specimens were cut randomly from the portions of bars remaining after the reinforcement had been cut to length for the beams. The tensile tests demonstrated consistent strength across all samples.

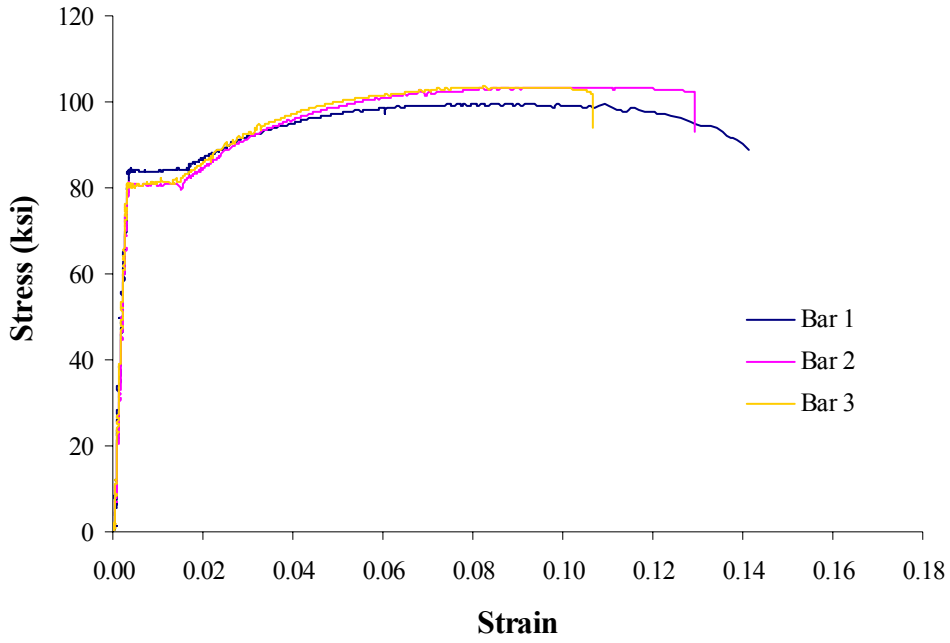

Figure 2.1 – Stress vs. Strain curves for all three No. 5 (No. 16) bar samples
Note: 1 ksi = 0.145 MPa

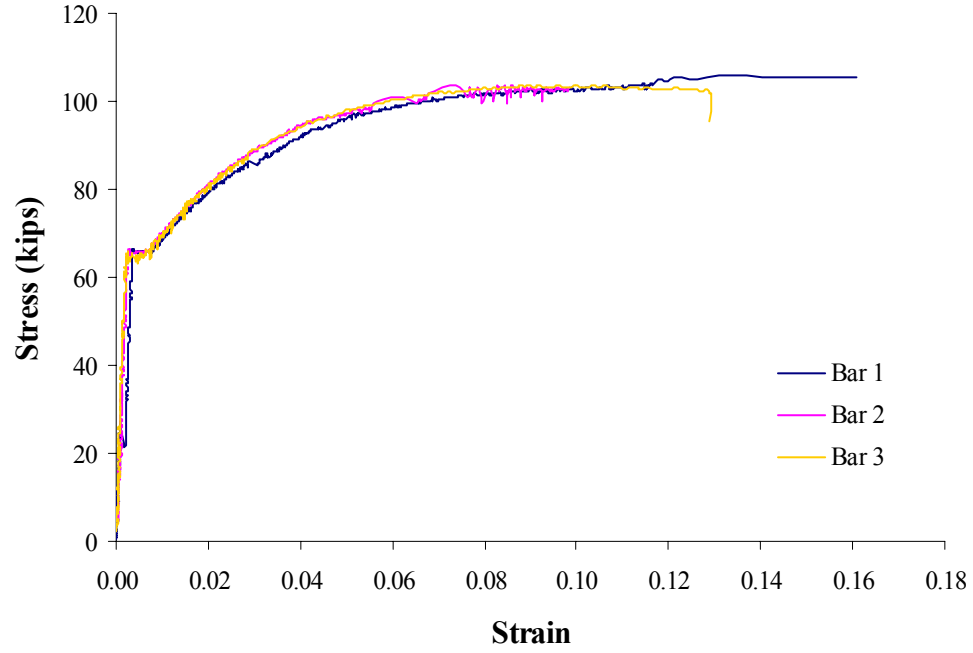

Figure 2.2 – Stress vs. Strain curves for all three No. 3 (No. 10) bar samples
Note: 1 ksi = 0.145 MPa

2.3 Blast Loading

2.3.1 Testing Configuration

The beams were subjected to blast loading in pairs, as shown in Figure 2.3. The two beams were placed on sand bags approximately 6 to 12 in. (150 to 300 mm) above the ground. The height of the sandbags was adjusted to level the beams (Fig. A.6 to A.9). The beams were placed parallel to each other, spaced 10 ft (3 m) apart, as measured from inside face to inside face, and connected using two 1½ in. (38 mm) diameter steel threaded rods. The rods were secured to the beams using 6 x 6 x 1 in. (150 x 150 x 25 mm) square steel washers and 1½ in. (38 mm) diameter nuts. The nuts and washers were tightened to both sides of each beam to ensure no slippage along the steel rods during the blast loading.

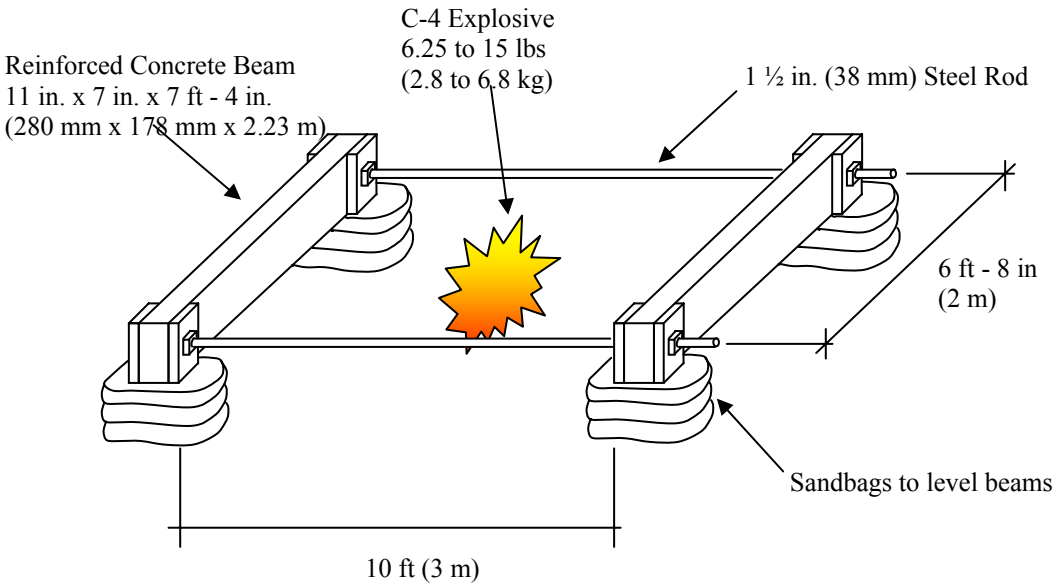

Fig 2.3 – Beam Blast Configuration

The interior face of both beams was painted using a white lime wash with the intent of aiding in the identification of cracks (Fig. A.10). This, however, did not work since the blast blew the lime off. The explosive charge was centered between the two beams and placed on sandbags so that the height of its centerline was roughly equal to the height of the beam centerline. The charge was double primed using both shock tubing and a time fuse to ensure detonation. The individual C-4 blocks were unwrapped from their individual block packaging and then tightly packed together to minimize air voids between blocks. The consolidated charge was then wrapped tightly with duct tape (Fig. A.11). The charge was constructed in such a manner as to have a reasonably symmetrical cross-section perpendicular to the beams to achieve similar blast loading on both (Fig. A.12). Charge weights of 10, 11.25, 15, and 6.25 lbs (4.54, 5.10, 6.80, and 2.83 kg) were used for beam sets, 1, 2, 3, and 4, respectively.

The threaded steel rods that connected the beams in each set appeared to work well. The permanent deflection in the beams caused the rods to bow in, as can be seen in Figure A.15. When the beam assembly was disassembled, the rods did not show any evidence of permanent deflection, indicating that they did not yield. Only one of the four sets of beams (Set 3) were blown off the sandbags that had been placed under the four corners of the beam assembly to level the beams (Fig. A.14).

2.3.2 Calculations of Anticipated Blast Load

Four pairs of beams were tested, each with a different weight of explosive. The forces on the interior beam face's were calculated using ConWep and are summarized in Table 2.6.

Table 2.6 – Anticipated blast load

Order of Test	**Beam Set**	**Charge Weight** lbs (kg)	**TNT Equivalent** lbs (kg)	**Peak Pressure** psi (MPa)	**Minimum Pressure** psi (MPa)	**Peak Impulse** psi-msec (MPa –msec)
1	3	15 (6.80)	19.2 (8.7)	2460 (17.0)	1156 (8.0)	399.2 (2.75)
2	2	11.25 (5.10)	14.4 (6.5)	1982 (13.7)	912 (6.3)	317.2 (2.19)
3	1	10 (4.54)	12.8 (5.8)	1794 (12.4)	823 (5.7)	288.8 (1.99)
4	4	6.25 (2.83)	8 (3.6)	1202 (8.3)	543 (3.7)	199.4 (1.37)

The ConWep program calculates the loading on the beam based on the assumption that the charge is level with the bottom edge of the beam. The charges used for the project were placed level with the centerline of the beams, about 5½ in. (140 mm) higher than the assumed charge location in ConWep. Locating the charge level with the center of the beams was done so that the loads along the top and bottom edges of the beam would be approximately equal and the maximum load would occur near the center of the face, as measured both horizontally and vertically. Placing the charge level with the bottom edge of the beam would have resulted in a larger pressure distribution and impulse load on the bottom edge of the beam than on the

top, with the maximum load at the bottom edge at the center of the face as seen in Figures C.1 and C.2.

The ConWep program was also used to calculate and graph the anticipated incident pressure history, anticipated reflected pressure history, anticipated incident and reflected pressure vs. range, and anticipated time of arrival and duration vs. range for all four charge weights. The anticipated incident pressure history graph illustrates how quickly the pressure dissipates after impacting the beam. In the case of the 15 lb (6.80 kg) charge, the total duration of the incident pressure is just 1.323 msec and for the 6.25 lb (2.83 kg) charge the pressure duration is 2.594 msec (Figs. C.3, C.7, C.11 and C.15). Figures C.4, C.8, C.12 and C.16 illustrate how quickly the anticipated reflected pressure impacts the beam and the duration of the reflected pressure for each of the charge weights. The anticipated incident and reflected pressure vs. range graphs show how quickly the incident pressure dissipates. In the case of the 15 lb (6.80 kg) charge, the incident pressure reaches 1 psi (6895 Pa) at 125 ft (38 m) from point of detonation (Figs. C.5, C.9, C.13 and C.17). The anticipated time of arrival and duration vs. range for each of the charges shows that the positive phase duration increases nonlinearly as the blast expands from the point of detonation (Figs. C.6, C.10, C.14 and C.18).

2.3.3 Blast Procedures

The beams were positioned for the tests on the day prior to the blast to prevent unnecessary delays on the range. Each set of beams was placed sufficiently far from

the others to ensure they would not receive damage from charges for the other sets. The charges were prepared by soldiers of the 70th Engineer Battalion in accordance with standard military demolition techniques, as defined in Field Manual 5-34, Field Manual 5-250, and unit specific standard operating procedures. M113 Armored Personnel Carriers were used for protection of personnel during detonation.

2.3.4 Actual Blast Loads

As stated in Section 1.3, the actual blast loading on the beams was not measured due to the limited nature of the project and the high cost of data acquisition instrumentation capable of measuring impulse loading.

2.3.5 Blast Variables

There are numerous factors that affect the actual impulse load that will strike a surface. Conceptually, the impulse load will expand in a uniform spherical shape from the point of detonation; that impulse force is the same at all points on the surface of the wave as it expands. While this is a necessary assumption in the calculation of anticipated impulse loads on a structure, it is not necessarily true. The distribution of impulse force on the expanding impulse wave is influenced by the shape and density of charge and objects that the impulse load comes in contact with as it expands. An additional variable that affects the impulse load experienced by the beams in this study is the portion of the blast load that is reflected by the ground. The reflected load increases the total blast force that strikes the beam. The extent of the reflected

impulse force reflected by the ground is influenced by how hard the ground is and how high the charge is above the ground at detonation. Softer ground will reduce the reflective force striking the beam. All four of the explosive charges used during this study were placed at approximately the same height above the ground on sandbags. Prior to detonation, the ground was not checked to determine its density.

2.4 FRP Repair

Beams 2B and 4A were repaired and strengthened using high strength repair mortar and two layers of FRP. Layer one provided flexural strengthening and layer two provided shear strengthening.

2.4.1 Materials Used

Fiber Reinforced Polymer

This project used the commercially available MBrace® Composite Strengthening System. The system is typically used in one of four ways: to upgrade load bearing capacities of concrete and masonry structures, to restore the capacity of concrete structures lost due to deterioration, to correct design or construction errors, and for seismic retrofit (MBrace 2002). The system was selected for its ease of installation, as described in Section 2.4.2. MBrace® High Strength Carbon Fiber fabric was used in this study. This fabric provides very high strength and stiffness relative to its weight, has excellent moisture and chemical resistance, and is highly resistant to fatigue and creep rupture (MBrace Design Guidelines 2002).

AMACO T430 Rapid Strength Repair Mortar

Beam 2B's spalling was greater than ¼ in. (6 mm) in depth and required the use of repair mortar. One batch of mortar was made with ½ in. (12.5 mm) maximum size limestone aggregate to repair spalling greater than 1 in. (25 mm) in depth (Table 2.7). A second batch of mortar was mixed without adding any aggregate for repair of spalling less than 1 in. (25 mm) in depth but greater than ¼ in. (6 mm) in depth (Table 2.8). The mortar was prepared and applied to the beam in accordance with the product label instructions. The mortar has a working time of approximately 45 min. at 72 ºF (22 ºC).

Table 2.7 – Rapid Strength Repair Mortar Proportions for spalling greater than 1 in. (25 mm)

Material	Proportions
AMACO T430 Mortar (1 bag)	55 lbs (25 kg)
Class 1, ½ in diameter max size limestone aggregate	25 lbs (11.3 kg)
Water	31.2 lbs (14.2 kg)

Table 2.8 – Rapid Strength Repair Mortar Proportions for spalling less than 1 in. (25 mm)

Material	Proportions
AMACO T430 Mortar (1 bag)	55 lbs (25 kg)
Water	31.2 lbs (14.2 kg)

Sika High Performance Anchoring Adhesive

An epoxy adhesive was injected in the large cracks on the outside face of Beam 2B (the side of the beam which went into tension during the blast loading). The beam was straightened by jacking it against an undamaged beam using threaded rods that were run through the same holes used to hold the beams together during the blast (Fig A.26). The epoxy adhesive was compressed in the cracks as they closed. The adhesive was applied in accordance with the packing instructions. The adhesive likely had little effect on the repaired beam because it only penetrated about 1 inch into the cracks.

2.4.2 Application Procedures

The application procedures vary depending on the specific commercial products used. Components from different products should not be combined. If this is done, the strength characteristics will change from those published by the product manufacturer. For this project, the application procedures followed the MBrace Standard Specifications (MBrace Design Guidelines 2002) and T430 Rapid Strength Repair Mortar package instructions.

Surface Preparation

The extent surface preparation depends on the extent of damage to the concrete. All unsound areas must be removed to expose sound concrete (Figs. A.23 and A.24). All areas of spalling and delamination greater than ¼ in. (6 mm) in depth

require the removal of the damaged concrete and replacement with a high strength repair mortar. The T430 mortar cannot be feathered and, therefore, requires that all seams between the mortar and existing concrete be cut to create a clean, smooth edge at least ½ in. (12 mm) in depth (Figs. A.28 to A.33). All uneven concrete protrusions must be ground smooth to a height of less than 0.04 in. (1 mm). All outside corners that will be covered by FRP must be rounded to a radius of no less than 0.5 in. (12 mm) (Fig. A.25). All cracks greater than 0.010 in. (0.25 mm) in width must be pressure injected with epoxy. Once repairs are completed and edges rounded, the beams are profiled by abrasive blasting (sandblasted) to remove any surface contaminates and prepare the surface for the epoxy primer (Fig. A.34 to A.36).

Primer

MBrace®Primer has a low viscosity to enable effective penetration of concrete pores. The primer consists of two separate components that are combined immediately prior to application. A single coat is applied using a short nap paint roller. Once the components are mixed, the working time is about 20 minutes at 77 ºF (25 ºC). The primer cured for approximately 18 hours, resulting in a clear, shiny, slightly tacky surface (Figs. A.37 to A.40).

Putty

MBrace®Putty is a high viscosity epoxy paste used to level the concrete surface after application of the primer. The putty consists of two components that are

combined using a mechanical mixer, in this case a drill driven paint mixing blade, for three minutes. Once mixed, the putty has a working time of about 40 minutes at 77 ºF (25 ºC). It is applied using a steel trowel. The putty cured for approximately six hours before the saturant was applied (Figs. A.41 to A.44).

FRP Application

Three basic methods of applying FRP to concrete have been developed. They are preimpregnation, where dry sheets of fiber and resin are laminated to the concrete, pultruded systems, where a fully cured FRP panel is attached to the concrete using an epoxy adhesive, and wet lay-up, where the fabric is saturated with the resin and then placed on the structure prior to curing. A modified wet lay-up method was used to repair the beams in this study. Instead of presaturating the fabric prior to placing it on the beams, as is done for many of the wet lay-up systems on the market, the fabric was saturated with the resin after being placed on the beams. The modified wet lay-up method is both simpler and easier since it does not require any specialized equipment (fiber saturation rollers) and can be done by one person. The fabric used was a carbon fiber fabric that came in a 24 in. (61 cm) wide role. Its mechanical properties of listed in Table 2.9. The fabric is easily cut to the required length using a common pair of scissors. The epoxy encapsulation resin used was Wabo®MBrace Saturant. The saturant consisted of two components that were combined just prior to use (Fig A.45). The resin is bright blue in color, and once mixed, the working time is about 45 minutes at 77 ºF (25 ºC).

Table 2.9 – Carbon Fiber Fabric Mechanical Properties (MBrace 2002)

MBrace Fiber	Ultimate Strength ksi (MPa)	Design Strength ksi (MPa)	Tensile Modulus ksi (GPa)
CF 130 High Tensile Carbon	620 (4275)	550 (3790)	33,000 (228)

The resin and fabric composite was applied to the beams by first placing an initial layer of resin on the bottom and sides of the beam using a medium nap roller [3/8 in. (10 mm) nap] (Fig A.46). The first layer of dry fiber was then placed on the resin and pressed smooth by hand to eliminate any wrinkles or air pockets. The first layer of fiber was a 2 x 6 ft (0.6 x 1.8 m) strip of fabric with the carbon fibers oriented parallel to the primary axis of the beam (Fig A.47). This layer of fabric provides tensile strength to the beam. Once smoothed and properly aligned, a generous second coat of resin was rolled onto the beam to saturate the fabric in place (Fig. A.48). The next layer of fabric was placed on top of this layer of resin. The second layer consisted of three 24 x 28 in. (610 x 710 mm) sheets and one 4 x 28 in. (100 x 710 mm) sheet. The sheets were oriented perpendicular to the primary axis of the beams to provide improved shear strength. The sheets were placed flush against each other and pressed smooth to eliminate any wrinkles or air pockets (Figs. A.49 and A.50). This layer of fabric was then covered with another generous layer of resin to ensure that it was fully saturated (Fig. A.51).

To apply the three layers of saturant and two layers of carbon fiber fabric took approximately 15 to 20 minutes per beam. After 24 hours, the beams were still tacky and by 48 hours they were tack free. The FRP takes seven days to reach its full load

carrying capacity according to the manufacturer but can begin receiving a load after just 24 hours (Fig A.52).

The MBrace (2002) Design Manual provides engineering properties on all components of the MBrace system. According to the design manual, the strength of the composite system is determined by using the net area of the carbon fiber fabric embedded in cured saturate. The carbon fiber fabric used in this study, MBrace CF 130, has a net area of 0.0065 $in.^2/in.$ (0.165 mm^2/mm). The design strength is determined by reducing the average strength by three standard deviations. The manual also provides the stress-strain curve for MBrace fibers (Fig 2.4).

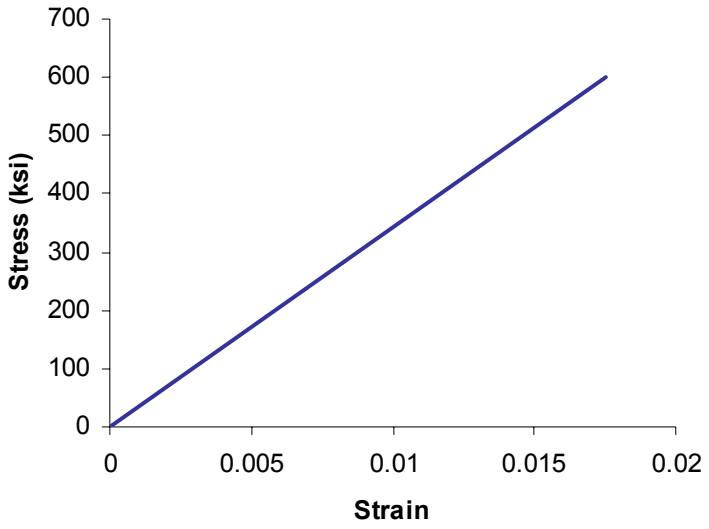

Fig. 2.4 – Representative stress-strain curve from tensile test data of MBrace CF 130 carbon fiber (MBrace 2002).
Note: 1 ksi = 0.145 MPa

2.4.3 Strength Increase due to FRP

The design approach used in determining flexural and shear strength increases due to the application of FRP is based on the MBrace Composite Strengthening

System Engineering Design Guidelines (MBrace 2002). All calculations are based on the assumption that the FRP is being applied to an undamaged beam. Since the FRP is applied to damaged beams in this study, the expectation is that the repaired beams will be unable to achieve the strength increase possible in an undamaged beam.

Flexural Strengthening

The cross sectional area of the flexural strengthening layer of FRP A_{FRP} was calculated to be 0.156 in.^{2} (100.6 mm^2) based on the carbon fiber thickness of 0.0065 in. (0.165 mm) and the sheet width of 24 in. (610 mm). However, not all the 0.156 in.^{2} (100.6 mm^2) contributes in increasing the flexural strength of the beam. The flexural strengthening FRP above the neutral axis does not provide any significant increase in strength when placed in compression. The second layer of FRP was not included in this calculation because its fibers run perpendicular to tensile force in the beam and, therefore, provide no additional flexural strength.

The iterative process used in Section 2.1.2 to design the beam was modified to include the FRP. Eq. (2.1) was modified to become Eq. (2.8).

$$A_s f_s + A_{FRPb} f_{FRPb} + A_{FRPs} f_{FRPs} = A_s^{'} f_s^{'} + 0.85 f_c^{'} \beta_1 cb \qquad (2.8)$$

Where A_{FRPb} = Cross sectional area of FRP along bottom of beam

f_{FRPb} = Stress in FRP along bottom of beam

A_{FRPs} = Cross sectional area of FRP on sides of beam below the neutral axis

f_{FRPb} = Stress in FRP on sides of beam below the neutral axis

A_{FRP} is recalculated for each iteration based on the location of the neutral axis to exclude any of the FRP that is in compression.

The effective depth d_{FRPs} at which the FRP on the sides act is determined based on the centroid of the strip in tension (Fig. 2.5).

The nominal moment capacity M_n is calculated using Eq. (2.9). Note that the top reinforcement is now in compression because $C > d'$; so the nominal moment capacity is

$$M_n = A_s f_s\left(d - \frac{c\beta_1}{2}\right) + A_s' f_s'\left(d' - \frac{c\beta_1}{2}\right) + A_{FRPb} f_{FRPb}\left(d_{FRPb} - \frac{c\beta_1}{2}\right) + A_{FRPs} f_{FRPs}\left(d_{FRPs} - \frac{c\beta_1}{2}\right) \quad (2.9)$$

The maximum total load P for the four point bending test is then determined using Eq. (2.6).

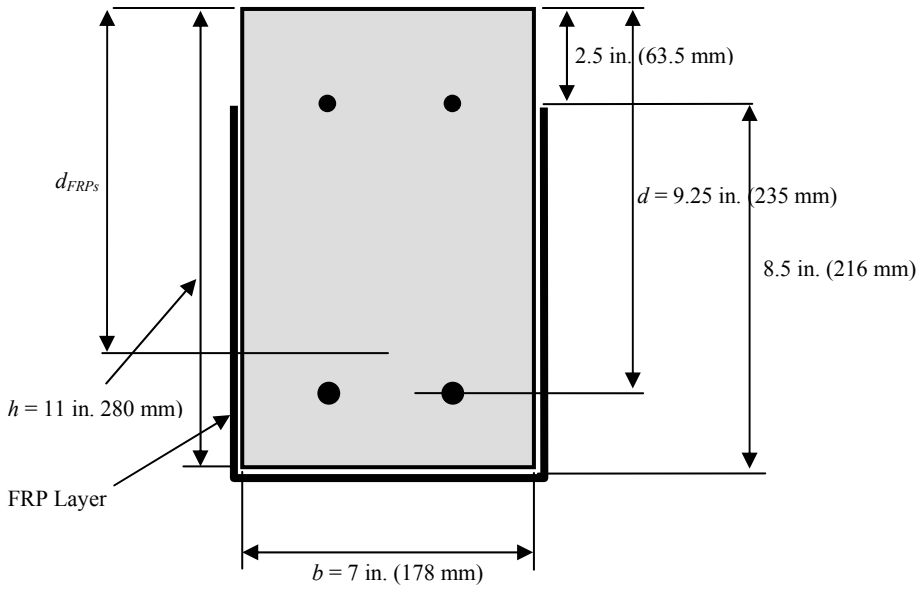

Fig 2.5 FRP Flexural Reinforcement Beam Cross Section

Based on these equations, the following FRP strengthened beam design properties were determined (Table 2.10). The actual material properties were determined through testing, as will be discussed in Sections 2.2.1 and 2.2.2.

Table 2.10 – FRP Strengthened Beam Section Properties

Material Properties Used in Calculation	f'_c psi (MPa)	f_y psi (MPa)	f_{FRPy} psi (MPa)	β_1	c in (mm)	M_n ft-kips (kN-m)	**Predicted maximum total load** lbs (kN)	f_{FRPb} **at failure** psi (MPa)
Design Properties	3500 (24)	60000 (414)	550000 (3790)	0.85	3.21 (81.5)	39.1 (53.1)	39060 (173.7)	240550 (1659)
Actual Material Properties	5160 (35.6)	82000 (565.4)	550000 (3790)	0.79	3.03 (77.0)	50.5 (68.6)	50550 (224.8)	260300 (1795)

The FRP reinforced beam's calculated nominal moment capacity represents a 40% increase over the non FRP reinforced nominal moment capacity of the beam using actual material properties, as calculated in Section 2.1.2.

The addition of the FRP results in an overreinforced section. The expected failure mode is calculated by comparing the strain in the FRP with the strain in the concrete at failure. The ultimate strain of the MBrace CF 130 carbon fiber is 0.017 and the ultimate strain of the concrete is 0.003, as set by ACI 318-02 Chapter 10.2.3. Equations (2.10), where failure is controlled by concrete crushing, and (2.11), where failure is controlled by FRP rupture, are used to determine failure mode (MBrace 2002). From these equations it is determined that the repaired beams should fail through crushing of the concrete.

$$\varepsilon_{fu} > \varepsilon_{cu}\left(\frac{h-c}{c}\right) \tag{2.10}$$

$$\varepsilon_{fu} < \varepsilon_{cu}\left(\frac{h-c}{c}\right) \tag{2.11}$$

Shear Strengthening

The total area of FRP shear reinforcement A_{fv} (in.^{2}) is determined using Eq (2.12). Continuous shear reinforcement was applied across the entire length of the beam beginning 6 in. (150 mm) from each end.

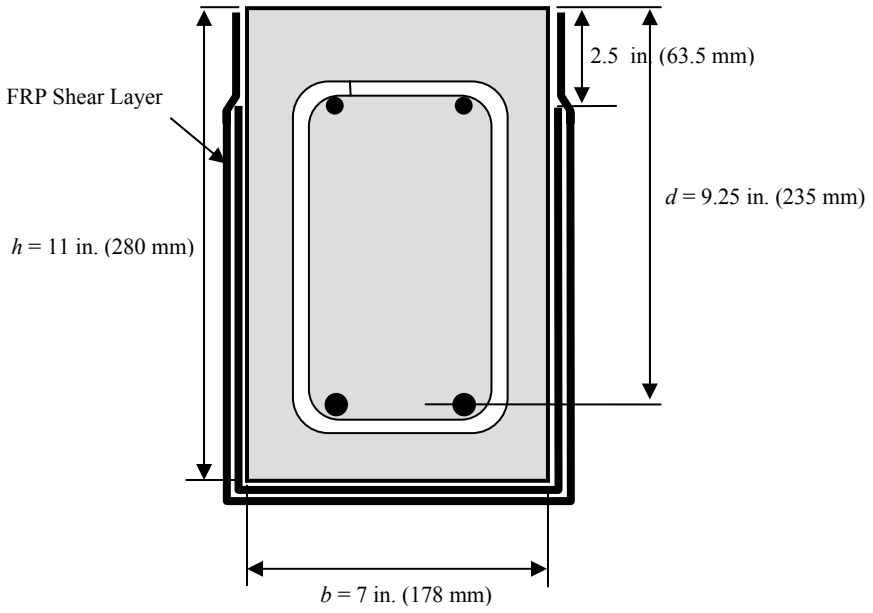

Fig 2.6 FRP Shear Reinforcement Beam Cross Section

$$A_{fv} = 2nt_f w_f \tag{2.12}$$

Where n = Number of plies of FRP shear reinforcement with fibers oriented in the primary direction

t_f = Thickness of one ply of FRP (for CF 130 t_f = 0.0065 in.)

w_f = Width of one strip of FRP shear reinforcement (in.)

The shear reinforcement was U-wrapped from the top edge on one side to the top edge on the other side for a total perimeter length of 29 in. (736 mm) (Fig. 2.6).

The additional shear capacity provided by the FRP, V_f, is calculated using Eq. (2.13)

$$V_f = \frac{A_{fv} f_{fe} (\sin\beta + \cos\beta) d_f}{s_f} \qquad (2.13)$$

Where f_{fe} = Stress level in the FRP shear reinforcement at failure based on a series of reduction factors to account for effective bond length, concrete strength, and wrapping scheme, as defined in MBrace (2002) Design Manual.`

β = Orientation of the primary fibers with respect to the longitudinal beam axis (for this study, β = 90 degrees)

d_f = Depth of shear reinforcement (for this study, d_f = 11 in.)

s_f = Spacing of the strips of FRP shear reinforcement (Continuous reinforcement was used to repair the beams in this study so $s_f = w_f$) (in.)

Total shear capacity of the beam with the addition of FRP is determined by Eq. (2.14) (MBrace 2002).

$$V_u = V_c + V_s + 0.85V_f \qquad (2.14)$$

Where V_c = Shear capacity of concrete

V_s = Shear capacity of reinforcing steel

Based on these equations, the following FRP shear strengthened beam design properties were determined (Table 2.11). The actual material properties were determined through testing, as discussed in Sections 2.2.1 and 2.2.2. With a calculated shear strength of 59.0 kips (262 kN), the shear strength should not govern the strength of the beams.

Table 2.11 – FRP Shear Strengthened Beam Section Properties

Material Properties Used in Calculation	f'_c psi (MPa)	f_{fe} psi (MPa)	f_y psi (MPa)	β degree	A_{fv} in.^{2} (mm^2)	V_f kips (kN)	V_u kips (kN)
Design Properties	3500 (24)	112500 (775)	60000 (414)	90	0.99 (637)	16.1 (71.6)	53.3 (237)
Actual Material Properties	5160 (35.6)	123000 (848)	66000 (455)	90	0.99 (637)	17.6 (78.2)	59.0 (262)

2.4.4 Anticipated Results

One of the risks incurred in using of FRP to strengthen a member is its inability to yield prior to failure. Much like unreinforced concrete, FRP will experience a brittle failure when the ultimate load has been reached. Typically, FRP will not fail before delamination has occurred between the concrete and the FRP. The delamination usually occurs between the surface concrete, which is bonded by the FRP primer epoxy, and the concrete immediately below the surface, which is not in contact with the epoxy. The beams in this study were expected to fail by delamination of the FRP reinforcement near the top center of the beams. An

additional potential failure mode is separation between the repair mortar and concrete due to poor surface preparation and/or failure to fully remove all damaged concrete. Delamination can also occur within the FRP due to excessive air voids and/or poor penetration of the resin into the fabric. Delamination of the epoxy putty from the primer or saturated fabric should not occur, but could, if either is not properly applied.

Chapter 3

Results and Discussion

3.1 Introduction

The concrete beam reinforcing cages and forms were built over the course of several weeks in July 2004. The beams were cast on August 13, 2004 and cured, as described in Section 2.1.4. The beams to be blast loaded were transported to Fort Riley on September 23, 2004, where they were offloaded on October 4 for demotion range set-up. On October 5, the beams were blast damaged, as described in Section 2.3. The beams were transported back to the University of Kansas on two separate hauls on October 5 and 7. The beams were repaired over the course of three weeks beginning on November 1. One beam from Set 2 (11.25 lb charge) and one beam from Set 4 (6.25 lb charge) were repaired using FRP. The two beams were sandblasted and a primer coat applied on 20 November. The putty and FRP were applied on 21 November. The primer, putty, and FRP were applied in the lab, with temperatures ranging from the low 60s to low 70s ºF (15 to 22 ºC).

3.2 Blast Damage Evaluation

3.2.1 Blast loads and Initial Visual Assessments

The beams were initially inspected immediately after the blast to determine if too much or too little damage had occurred, so that the quantity of explosives could be adjusted on subsequent blasts. Set 3 was tested first using 15 lbs (6.8 kg) of C-4. This

resulted in significant damage to the concrete and yielding of the steel. The blast caused permanent horizontal deflections of 2 ½ and 3 in. (64 and 76 mm) on the two beams.

Set 2 was tested next using 11.25 lbs (5.10 kg) of C-4. This charge also resulted in damage to the concrete and yielding of the steel, but at a lesser degree than the first blast. The resulting damaged was within the range of what appeared to be potentially repairable. The blast caused permanent horizontal deflections of 1½ in. (38 mm) on the two beams.

For the third blast (Set 1), the charge was reduced to 10 lbs (4.54 kg) in an attempt to cause cracking in the beam without causing yielding in the steel. The resulting damage was nearly as great as the damage caused by the 15 lb (6.80 kg) charge. Upon inspection of the ground beneath the charge, it became clear the ground was significantly harder than that beneath the 11.25 lb (5.10 kg) charge. The harder ground would have caused a larger reflective load to strike the beam, and it is the likely cause of the greater damage, despite having a lower charge weight. The blast caused permanent horizontal deflections of 2½ and 3 in. (64 and 76 mm) on the two beams

The fourth and final blast (Set 4) used only 6.25 lbs (2.83 kg) of C-4. This resulted in flexural cracking through the beams at several locations but no apparent yielding of the steel. Neither beam had any permanent horizontal deflection after the blast.

3.2.2 Damage Assessment and Crack Patterns

The damage inflicted on the two beams of each set of blast damaged beams was similar but not the same. Therefore, the comparison between the repaired and the

unrepaired beam in each set should only be viewed as providing a general range of strength improvement, not as a hard percentage of what can be obtained for other damaged and repaired beams.

The damage experienced by each beam is presented in greater depth on the damage assessment worksheets in Appendix B. The damage assessment worksheets also include sketches that illustrate the cracking and spalling that the beam experienced. As can be seen in Figures B.1 through B.8, the crack patterns show that the beams experienced both flexural and shear cracking in the lateral direction, as well as crushing of the concrete at the center of the inside face of the beams for all of the beams, except those damaged by the 6.25 lb (2.83 kg) charge. For Sets 1 and 3 [10 lb and 15 lb (4.54 and 6.80 kg) charges], the cracking was so extensive that no sound concrete remained in the middle of the beams. As a result, only the beams in Sets 2 and 4 [6.25 and 11.25 lb (2.83 and 5.10 kg) charges] were repaired with FRP.

3.2.3 Failure Mechanisms

Six of the eight beams failed due to the blast load. The reinforcement in the six beams appears to have yielded followed by crushing of the concrete on the front face. The areas of crushed concrete exposed portions of the reinforcement in all six beams. The beams experienced both shear and flexural cracking extending through the entire cross section of the beams. The cracks on the back side of the beams were splayed open due to permanent deformation. Some of the large cracks ranged from 0.1 to 0.3 in. (2.5 to 7.5 mm) gap. Several of the beams lost chunks of concrete on the back side due to the

extensive cracking in the center of the beams. None of the beams experienced any permanent vertical deflection.

3.3 Beam Flexure Test

3.3.1 Instrumentation

The beams were tested in third-point loading on a 120 kip (534 kN) Baldwin Universal Testing Machine (Fig. A.53). The total force applied and deflection was measured every ½ sec. using a load cell and displacement transducer connected to a data acquisition system (Fig. A.54).

3.3.2 Test Procedure

Each beam was mounted in the reaction frame on the universal testing machine and centered under the top reaction surface. The beam rested on two 2 in. (50 mm) diameter steel rods spaced 6 ft (1.83 m) apart and 3 ft (0.915 m) from the center of the beam. The rods were allowed to freely rotate, inhibited only by a small bead of clay on either side to prevent the rods from rolling off the plates on which the sat. On the top of the beam, two 2 in. (50 mm) diameter steel rods spaced 2 ft (0.61 m) apart and 1 ft (0.305 m) from the center of the beam. A steel beam was placed on top of the rods to transfer the load from the top reaction surface to the rods. The rods were allowed to freely rotate, inhibited only by a small bead of clay on either side to prevent the rods from rolling off the top of the beam.

The load was applied to the beams at approximately 150 lb/s (670 N/s) until failure was reached. The two control beams (C1 and C2) were tested first, followed by

the two unrepaired beams (2A and 4B). The two repaired beams (2B and 4A) were then tested. All six beams yielded good test results. Beams 1A, 1B, 3A and 3B were beyond reasonable repair and were not tested in third-point loading.

Beam 2B had a camber of 0.313 in. (7.95 mm) at its center prior to loading. Additionally, the full width of the beam at each end was not fully resting on the steel bearing rollers due to the slight torque in the beam. Following the application of the first several thousand pounds of load the beam appeared to be fully seated, with no visible torque or chamber.

3.3.3 Comparison of flexural strength

All six beams ultimately failed when the concrete at the top center of the beams crushed. In the case of the two control beams (C1 and C2) and beam 4B (unrepaired with minor damage), the beams began to behave nonlinearly at 85% to 90% of their ultimate load (Fig. 3.1). Both FRP repaired beams (2B and 4A) demonstrated a significant increase in strength. Beams 2B and 4A provided, respectively, 26% and 45% greater load carrying capacity than their unrepaired counterparts.

The two control beams (C1 and C2) and the unrepaired beam 4B had similar load vs. deflection curves (Fig. 3.1) and maximum load at failure (Table 3.1). Beam 4B achieved 93.5% of the average strength of the two control beams.

Repaired beam 2B had about the same strength as beams C1, C2 and 4B, but had a significantly lower stiffness at low loads. Beam 2B did not experience any significant nonlinear behavior prior to failure (controlled by crushing of concrete). The low stiffness over the first 0.3 in. (7.6 mm) of deflection was likely caused by a combination of several

factors, which are discussed in Section 4.1.2. Beam 2A, the most significantly damaged of the two unrepaired beams, deflected at about twice the rate of the other beams and showed some nonlinear behavior prior to failure. It failed at 75% of the average strength of the two control beams, C1 and C2.

The final beam tested was 4A. It had had through cracking of the concrete but no yielding of the steel from the blast load. It was repaired with the FRP and was 36% stronger than the average of the two control beams. It was also stiffer than the control beams and only demonstrated modest yielding before reaching failure due to crushing of concrete and delamination of the FRP in the center (Fig. A.55).

Table 3.1 – Load test results

Beam Identifier	**Beam type**	**Predicted maximum total load** lbs (kN)	**Maximum total load** lbs (kN)	**Approx. load at initiation of nonlinear behavior** lbs (kN)	**Deflection at failure** in (mm)
C1	C	36400 (161.9)	41900 (186.4)	35000 (155.7)	1.04 (26.4)
C2	C	36400 (161.9)	41500 (184.6)	35000 (155.7)	0.95 (24.1)
2A	D	36400 (161.9)	31175 (138.7)	N/A	1.06 (26.9)
2B	D+R	50550 (224.8)*	39350 (175.0)	N/A	0.84 (21.3)
4A	D+R	50550 (224.8)*	56700 (252.2)	46000 (204.6)	0.93 (23.6)
4B	D	36400 (161.9)	39000 (173.5)	36000 (160.1)	1.03 (26.2)

C – Control
D – Damaged
R – Repaired
* Predicted maximum value had the beam been undamaged with FRP reinforcement added (Section 2.4.3).

Both repaired beams showed a significant improvement in strength in comparison with their unrepaired counterpart. Beam 2B was 26% stronger than Beam 2A and Beam 4A was 45% stronger than Beam 4B.

All beams, with the exception of 2B and 2A, exhibited strengths that were greater than predicted (Table 3.1), and for 2B, the repairs still allowed 94 % of the average capacities of beams C1 and C2 to be achieved.

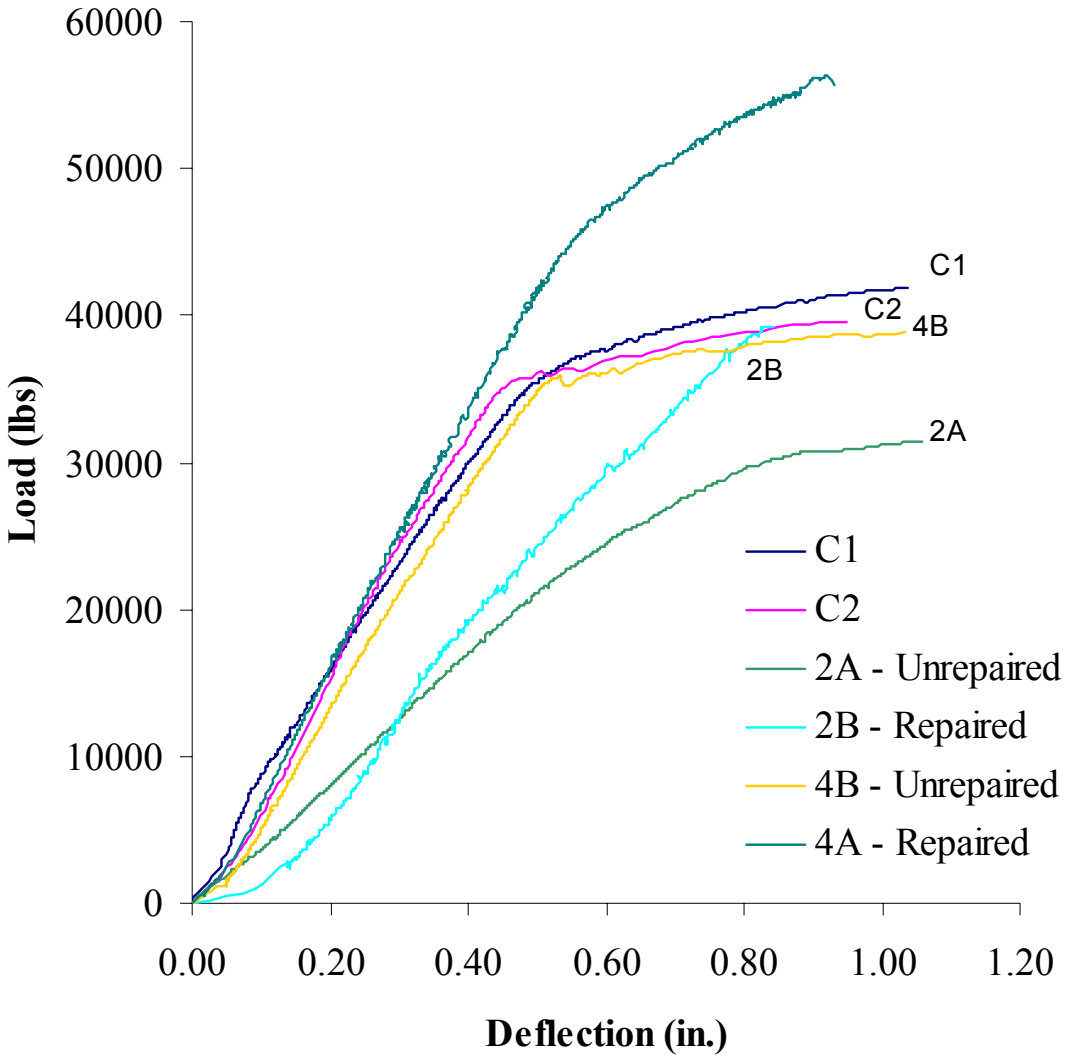

Figure 3.1 – Combined Load vs. Deflection curves for the six third-point load tested beams.
Note: 1 in. = 25.4 mm

Chapter 4

Summary and Conclusions

4.1 Summary

4.1.1 Overview of Project

A series of six tests were conducted on reinforced concrete beams to determine if FRP repair of blast damaged concrete beams was a viable means of regaining lost flexural strength in a damaged member. Four sets of two beams each were damaged through the use of high explosives. Two of the four sets of beams (Sets 1 and 3) were determined to have received damage too high for reasonable repair. Of the remaining two sets of beams, one set, Set 2, experienced serious damage to include yielding of the steel reinforcement, significant cracking of concrete, and crushing of concrete, resulting in a permanent horizontal deflection. The other set of beams, Set 4, received less significant damage with no yielding of the steel or crushing of concrete and only cracking through the cross section of the beam in several locations.

Beams 2B and 4A were repaired using two layers of FRP applied along both sides and the bottom of the beam. The FRP provided both flexural and shear reinforcement to the beams. For beam 2B, the unsound concrete was removed and replaced with high strength repair mortar.

The two control beams (C1 and C2), two damaged and unrepaired beams (2A and 4B), and the two FRP repaired beams (2B and 4A) were tested to failure in third-point bending.

Results from the tests provided information about the behavior of the repaired and unrepaired beams in comparison with control beams. Beam demensions, reinforcement

and concrete were kept constant. The cross section was 7 x 11 in. (178 x 280 mm) (Fig. 2.1). The 28 day compressive strength of the concrete used in the specimens was 4260 psi (29.4 MPa). The concrete strength at the time of the blast loading was 4770 psi (32.9 MPa) and at the time of the strength tests was 5160 psi (35.6 MPa).

The longitudinal reinforcement consisted of two No. 5 (No. 16) bars. The measured yield strength of the longitudinal reinforcement was 82 ksi (716 MPa) (Table 2.4). The top reinforcement, which in reality was in tension falling a fraction of an inch below the neutral axis of the beams, consisted of two No. 3 (No. 10) bars. The measured yield strength of the compression reinforcement was 66 ksi (455 MPa) (Table 2.4). A total of 22 stirrups were placed 4 in. on center over the entire length of the beam. The stirrups were made from the same No. 3 bar as the top reinforcement.

Third-point loading was applied to the beams using a 120 kip hydraulic universal testing machine. The beam deflection and loading were measured up to the point of flexural failure.

4.1.2 Observed Behavior

Blast Loading

Damage to the beams was not directly proportioned to the weight of the explosive charge used on each set of beams. In general, the higher the weight of the charge the greater the damage. However, this did not always hold true. Beam Set 1 was damaged using 10 lb (4.54 kg) of C-4 and received more extensive damage to both beams than Set 2, which was damaged using 11.25 lb (5.10 kg) of C-4. This was likely due to several factors, but most notably the ground appeared to be much harder under Set 1 than Set 2,

as was evident by the size of the crater below the charge. Firmer ground would have caused a larger reflected blast load to strike Set 1 than stuck Set 2, thereby causing more damage.

The threaded steel rods that connected the beams in each set appeared to work well. The permanent deflection in the beams caused the rods to bow in as can be seen in Figure A.15. When the beam assembly was disassembled the rods did not show any evidence of permanent deflection, indicating that they did not yield. Only one of the four sets of beams (Set 3) were blown off the sandbags that had been placed under the four corners of the beam assembly to level the beams (Fig. A.14). Use of lime whitewash which was painted on the inside beam face prior to blast loading to help identify cracking was ineffective since it was blown off the beam by the blast.

Flexural Capacity

Six beams were tested in third-point loading to determine their flexural capacity. All six beams ultimately failed when the concrete at the top center of the beams crushed. In the case of both control beams and beam 4B (unrepaired with minor damage), the beams began to deform in a nonlinear manor at approximately 85% to 90% of there ultimate load (Fig. 3.1). Both FRP repaired beams (2B and 4A) demonstrated a significant increase in strength. Beams 2B and 4A, respectively, provided 26% and 45% greater load carrying capacity than there unrepaired counterparts respectably. However, both FRP repaired beams demonstrated little or no yielding prior to reaching failure.

4.1.3 Effect of Test Variables

The weight of explosive charge used significantly influenced the damage caused to the beams. However, the damage inflicted on the two beams of each set of blast damaged beams was similar but not the same. Therefore, the comparison between the repaired and unrepaired beam of each set should only be viewed as providing a general range of strength improvement, not as a hard percentage of what can be achieved for other damaged and repaired beams.

The extent of damage significantly influenced the beams' flexural capacity both of the repaired and unprepared beams. In both cases the repaired beams performed significantly better than the unrepaired beams.

4.1.4 Evaluation of Test Results

Load-deflection curves were plotted for the six beams tested to failure. These curves were combined on a single graph to illustrate the differences in performance between the beams.

4.2 Conclusions

The conclusions drawn from these tests provide general insight into the effects of FRP in blast damage repair. More tests would be needed to develop a precise range of strength improvement in repaired beams.

1. Fiber reinforced polymer represents a viable option for the repair of blast damaged beams. The FRP repaired beams demonstrated a significant

improvement in flexural capacity in comparison to their equivalently damaged counterparts.

2. Even carefully centered explosive charges will not yield identical damage to two beams that are blast loaded as done in this study.
3. Blast damaged beams can be repaired even after experiencing flexural and shear cracking, crushing of concrete, and yielding of reinforcement.
4. FRP is a relatively simple and easy repair system to install.
5. The addition of FRP to beams can result in an overreinforced section, thereby preventing any significant yielding prior to a brittle fracture of the concrete.

References

ACI Committee 318, 2002, *Building Code Requirements for Structural Concrete* (ACI 318-02) and *Commentary* (ACI 318R-02), American Concrete Institute, Detroit.

ASTM A 615, "Standard Specification for Deformed and Plain Billet-Steel Bars for Reinforced Concrete, American Society for Testing and Materials," Philadelphia, PA.

ASTM C 39, "Compressive Strength, American Society for Testing and Materials," Philadelphia, PA.

ASTM C 496, "Splitting Tensile Strength, American Society for Testing and Materials," Philadelphia, PA.

Barakat, M. and Hetherington, J., 1999, "Architectural Approach to Reducing Blast Effects on Sructures," Paper 11796, *Proceedings of the Institution of Civil Engineers*, Structures and Buildings, Nov., pp. 333-343.

Cabridenc, P. and Garnero, P., 1992, "Computation of the Warhead Blast Effect on a Structure: Experimental Validation," *Structures Under Shock and Impact II*; Proceedings of the Second International Conference, Portsmouth, U.K., 16-18 June, pp. 555-570.

Caldwell, T., 1999, "Bomb Blast Damage to a Concrete-Framed Office Building – Ceylinco House – Columbo, Sri Lanka," *Structures Congress Proceedings*, pp. 602-605.

ConWep 2.1.0.3, US Army Corps of Engineers Engineering Research and Development Center Geotechnical/Structures Laboratory, Vicksburg, MS.

Eytan, R., 1992, "Response of Real Structures to Blast Loading – the Israeli Experience," *Structures Under Shock and Impact II: Proceedings of the 2nd International Conference*, Portsmouth, U.K., 16-18 June, pp. 483-495

FM 5-34 - Engineer Field Data, 2004, Department of the Army Field Manual, HQ Dept. of the Army, Washington, DC, 16 Jan.

FM 5-250- Explosives and Demolitions, 1999, Department of the Army Field Manual, HQ Dept. of the Army, Washington, DC, 30 June.

Hamad, B.S., 1993, "Evaluation and Repair of War-damaged Concrete Structures in Beirut," *Concrete International: Design and Construction*, v 15, n 3, Mar., pp. 47-51.

Kachlakev, D., Green, B., and Barnes, W., 2000, "Behavior of Concrete Specimens Reinforced with Composite Materials – Laboratory Study," Oregon Department of Transportation, Report SPR 387, Feb.

Krauthammer, T. and Zineddin. M., 1999, "Structural Concrete Slabs under Localized Impact," Proc. 9th International Symposium on Interaction of the Effects of Munitions with Structures, Berlin, Germany, 3-7 May.

James, J., Wood, T., Kruse, E., and Veatch J., 2001 "Vehicle Bomb Blast Effects and Countermeasures," *35th Annual IEEE International Carnahan Conference on Security Technology*, 16-19 Oct.

MBrace® Composite Strengthening System Engineering Design Guidelines, 3rd ed., 2002, Watson Bowman Acme Corp.

Mlakar, P. F., Corley, W., Sozen, M., and Thornton, C., 1998, "The Oklahoma City Bombing: Analysis of Blast Damage to the Murrah Building," *Journal of Performance of Constructed Facilities*, v 12, n 3 Aug., pp. 100-112.

Ninni, A. and Gold, W., 1998, "Strength Assessment of External FRP Reinforcement," *Concrete International*, v 20, n 6, June, pp. 39-42.

Ramabhushanam, E. and Lynch, M., 1994, "Structural Assessment of Bomb Damage for World Trade Center," *Journal of Performance of Constructed Facilities*, v 8, n 4, Nov., p 299-242.

Schleyer, G.K. and Hsu, S.S., 2000, "A Modeling Scheme of Predicting the Response of Elastic-plastic Structures to Pulse Pressure Loading." *International Journal of Impact Engineering*, v 24, n 8, p 759-777.

Teng, Chan, Smith, and Lam, 2002, *FRP Strengthened RC Structures*, John Wiley and Sons, Ltd., New York, NY.

TM 5-855-1 - Fundamentals of Protective Design for Conventional Weapons, 1986, Department of the Army Technical Manual, HQ Dept. of the Army, Washington, DC 3 Nov.

TM 5-1300 - Structures to Resist the Effects of Accidental Explosions (with Addenda), 1990, Department of the Army Technical Manual, Department of the Navy Publication (NAVFAC P-397), Department of the Air Force Manual (AFM 88-22), Washington, DC, 19 Nov.

Walley, F., 1994, "The Effect of Explosions on Structures," Structural and Building Board, Building Panel Paper 10469, *Proceedings of the Institution of Civil Engineers, Structures and Buildings*, Aug., pp. 325-334.

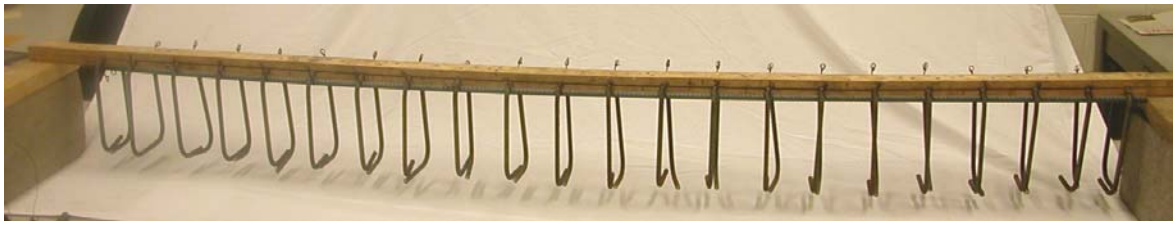

Figure A.1 - No. 3 (No. 10) bar stirrups mounted in wood jig to ensure 4 in. (100 mm) center to center spacing is maintained during the reinforcing cage construction.

Figure A.2 – Reinforcing cage with horizontal reinforcement wire tied to stirrups, prior to the removal of the wood spacing jig.

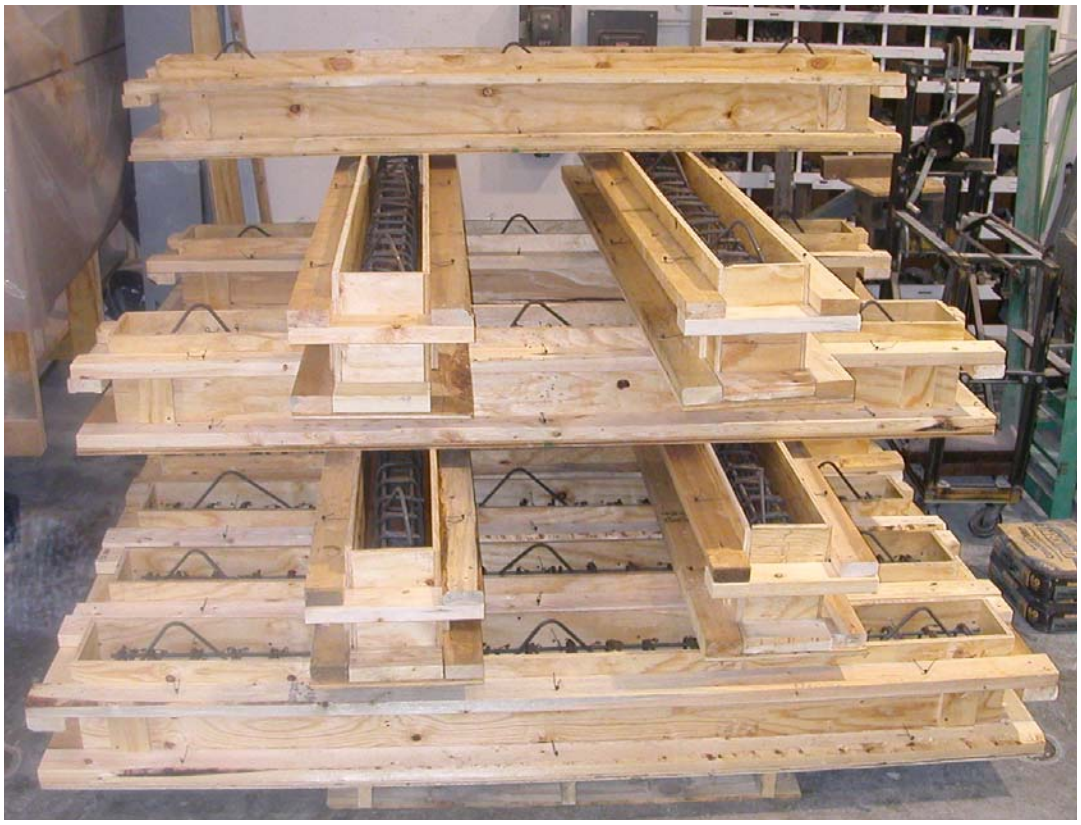

Figure A.3– Storage of forms with reinforcement cages mounted inside.

Figure A.4 – Forms prior to placement of concrete.

Figure A.5 – Forms were covered with wet burlap following the placement of the concrete to ensure proper curing.

Figure A.6 – Beam blast configuration for Set 1

Figure A.7 – Beam blast configuration for Set 2

Figure A.8 – Beam blast configuration for Set 3

Figure A.9 – Beam blast configuration for Set 4

Figure A.10 – Interior face of beams were painted using lime and water to more easily identify cracks. This, however, did not work since the blast blew the lime off.

Figure A.11 – The C-4 charge was dual primed and tightly packed into a single large charge for each blast. The charge was tightly wrapped with military issue green duct tape to minimize air voids within the charge.

Figure A.12 – The C-4 charge was placed in an empty sandbag to protect it during transport from charge assembly area to the blast site. The charge was centered between the two beams and placed on sandbags to make it approximately level with the centerline of the two beams.

Figure A.13 – The C-4 charges were detonated from behind the safety M113 Armored Personnel Carriers which were located approximately 450 ft (135 m) from the blasts

Figure A.14 –Set 3 following detonation of 15 lbs (6.80 kg) (12 blocks) of C-4

Figure A.15 –Set 3 following detonation of 15 lbs (6.80 kg) of C-4. Note the inward bow in the steel rod, following the blast, due to yielding of the concrete beams. A similar bow in the steel rod was observed on Sets 1 and 2 following their blasts.

Figure A.16 – Beam 3B following detonation of 15 lbs (6.80 kg) of C-4. Note the outward bend due to the yielding of the concrete beams.

Figure A.17 –Set 2 following detonation of 11.25 lbs (5.10 kg) (9 blocks) of C-4

Figure A.18 – Beam 2B following detonation of 11.25 lbs (5.10 kg) of C-4. Note the outward bend due to the yielding of the concrete beams.

Figure A.19 –Set 1 following detonation of 10 lbs (4.54 kg) (8 blocks) of C-4

Figure A.20 – Beam 1B following detonation of 10 lbs (4.54 kg) of C-4. Note the outward bend due to the yielding of the concrete beams.

Figure A.21 –Set 4 following detonation of 6.25 lbs (2.83 kg) (5 blocks) of C-4

Figure A.22 – Beam 4B following detonation of 6.25 lbs (2.83 kg) of C-4. Note that the beam appears straight with no outward sign of yielding of the reinforcement within the beam.

Figure A.23 – The beams were all brought back to the lab where the crushed concrete was removed using a hammer and chisel. This is the inside face of beam 3B after all crushed concrete has been removed.

Figure A.24 –This is the outside face of beam 3B after all loose concrete has been removed.

Figure A.25 – The bottom edges of beams 4A and 2A were rounded to a ½ in. (13 mm) diameter radius to reduce the force concentration on the FRP which wraps perpendicular across the edge.

Figure A.26 – Beam 2A was straightened by jacking it against an undamaged beam using threaded rods that were run through the same holes used to hold the beams together during the blast. The large cracks on the outside face of the beam were filled with epoxy adhesive prior to jacking the beam straight.

Figure A.27– Top view of Beam 2A after it has been straightened. The dark gray lines are from the epoxy that had been injected into the large cracks prior to straightening.

Figure A.28 – The edges around the area in which the high-strength repair mortar was to be placed were cut ½ in. (13 mm) deep using a masonry blade on a skill saw.

Figure A.29 – The area within the cut edges was scrubbed using a wire brush and pressurized air to ensure it was free of any loose material prior to placing the repair mortar.

Figure A.30 – Beam 2A after the repair mortar has cured. Because the damaged area was greater than 1 in. (25 mm) in depth, ½ in. (13 mm) max size limestone aggregate was added to the mortar. Note the beam still has remaining damage at the center of the bottom edge and on the right side of the top front edge.

Figure A.31 – The damage on the right side of the top front edge in Figure A- 30 was cut out the same way using a masonry blade on a skill saw.

Figure A.32 – The damage at the center of the bottom edge from Figure A- 30 after being cut out.

Figure A.33 – The repaired damage of the edge used high-strength repair mortar without any aggregate added. The vertical spalling damage that remains was repaired using the epoxy putty because it was less than ¼ in. (6 mm) in depth.

Figure A.34 – Beams 2A and 4A were sandblasted prior to application of the FRP Primer to remove any surface contaminates and prepare the surface for the epoxy primer. Safety precautions, to include no exposed skin and wearing of a hood, must be taken when sandblasting.

Figure A.35 – Beam 4A after surface preparation but before the application of the primer.

Figure A.36 – Beam 2B still had a slight bow in it after the straightening process had been completed. Beam 4A can be seen in the back ground.

Figure A.37 – The MBrace Primer comes in two parts that are mixed just prior to use. Once mixed, there is about 20 minutes working time prior to setting.

Figure A.38 – One coat of MBrace Primer was applied to each beam using a short nap roller

Figure A.39 – The primer cured for approximately 18 hours resulting in a clear, shiny, slightly tacky surface.

Figure A.40 – The repaired portion of beam 2A could be clearly seen after the primer coat was applied.

Figure A.41 – The MBrace Putty comes in two parts that are mixed just prior to use. Once mixed, there is about 40 minutes working time prior to setting.

Figure A.42 – The MBrace Putty has a high viscosity and is applied using a steel trowel.

Figure A.43 – The MBrace Putty is applied in a thin coating to smooth the surface of the beam.

Figure A.44 – The MBrace Putty cured for approximately six hours before the saturant was applied.

Figure A.45 – The MBrace Saturant comes in two parts that are mixed together just prior to use. Once mixed, there is about 45 minutes working time prior to setting.

Figure A.46 –The MBrace Saturant was applied to each beam using a medium nap roller.

Figure A.47 –The first layer of carbon fiber fabric was applied running parallel to the beam's primary axis. This layer of fabric provided tensile reinforcement to the beams.

Figure A.48 –The MBrace Saturant was applied on top of the fabric using a medium nap roller. The saturant was applied generously to ensure that the fabric was fully saturated.

Figure A.49 – The second layer of carbon fiber fabric was applied on top of the fully saturated longitudinally oriented fabric. The second layer of fabric ran perpendicular to the beam's primary axis to provide shear reinforcement.

Figure A.50 – The fabric was smoothed to remove all air voids beneath it and the previous layers. Care was also taken to ensure the fibers in the fabric remained straight and properly oriented.

Figure A.51 – A final layer of saturant was applied to the beams on top of the shear reinforcement fabric. The saturant was applied generously to ensure the fabric was fully saturated.

Figure A.52 – To apply the three layers of saturant and two layer of carbon fiber fabric took approximately 15 to 20 minutes per beam. After 24 hours the beams were still tacky and by 48 hours they were tack free. The FRP takes seven days to reach its full load carrying capacity according to the manufacturer but can begin receiving a load after just 24 hours.

Figure A.53 – Beam 2A mounted in the third-point reaction from on the 120 kip (534 kN) Baldwin Universal Testing Machine.

Figure A.54 – Displacement transducer measured the deflection of the centerline of the beam. The horizontal bar was epoxyed to the side of the beam and the transducer rod was firmly attached to the bar with two nuts. The transducer had a 2 in. (50 mm) displacement capacity.

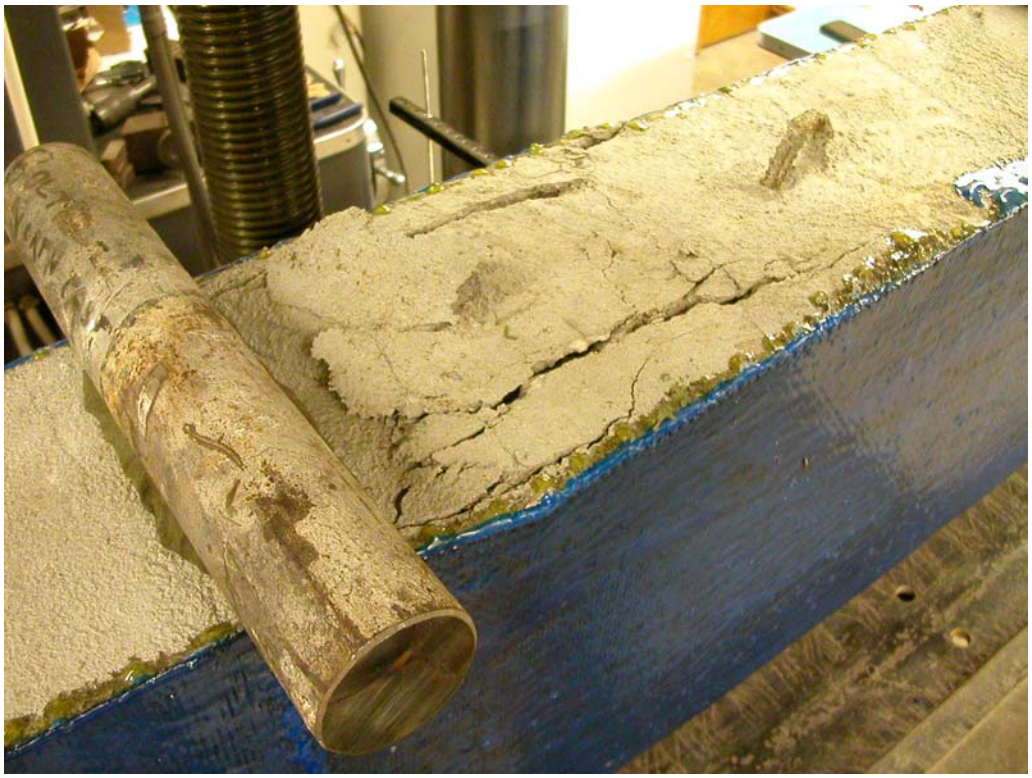

Figure A.55 – Compression failure in the concrete of beam 4A after reaching a load of 56,700 lb (252.2 kN) in third-point loading.

Beam Designation: 1A

Explosives Used: 10 lbs (4.54 kg) of C-4 **Face-to-Face Spacing of Beams:** 10 ft (3 m)

Description of Damage: The beam experienced extensive cracking and deformation due to the blast load. The reinforcement yielded and approximately 140 in.^{2} (90000 mm^2) of the front surface was crushed and removed by the blast. The crushed surface revealed the full height of stirrup No. 11 and the lower half of stirrup No. 12. A short length of the tensile reinforcement between the stirrups was exposed on the front face. The beam experienced through cracking along nearly its entire length, with cracks every 4 to 8 in. (100 to 200 mm). Shear cracks are seen towards the middle of the beam and flexure cracks near the ends.

Deformation: 2.5 in. (64 mm) **Crater Size in Soil:** 2 ft (0.6 m)

Beam Sketch:

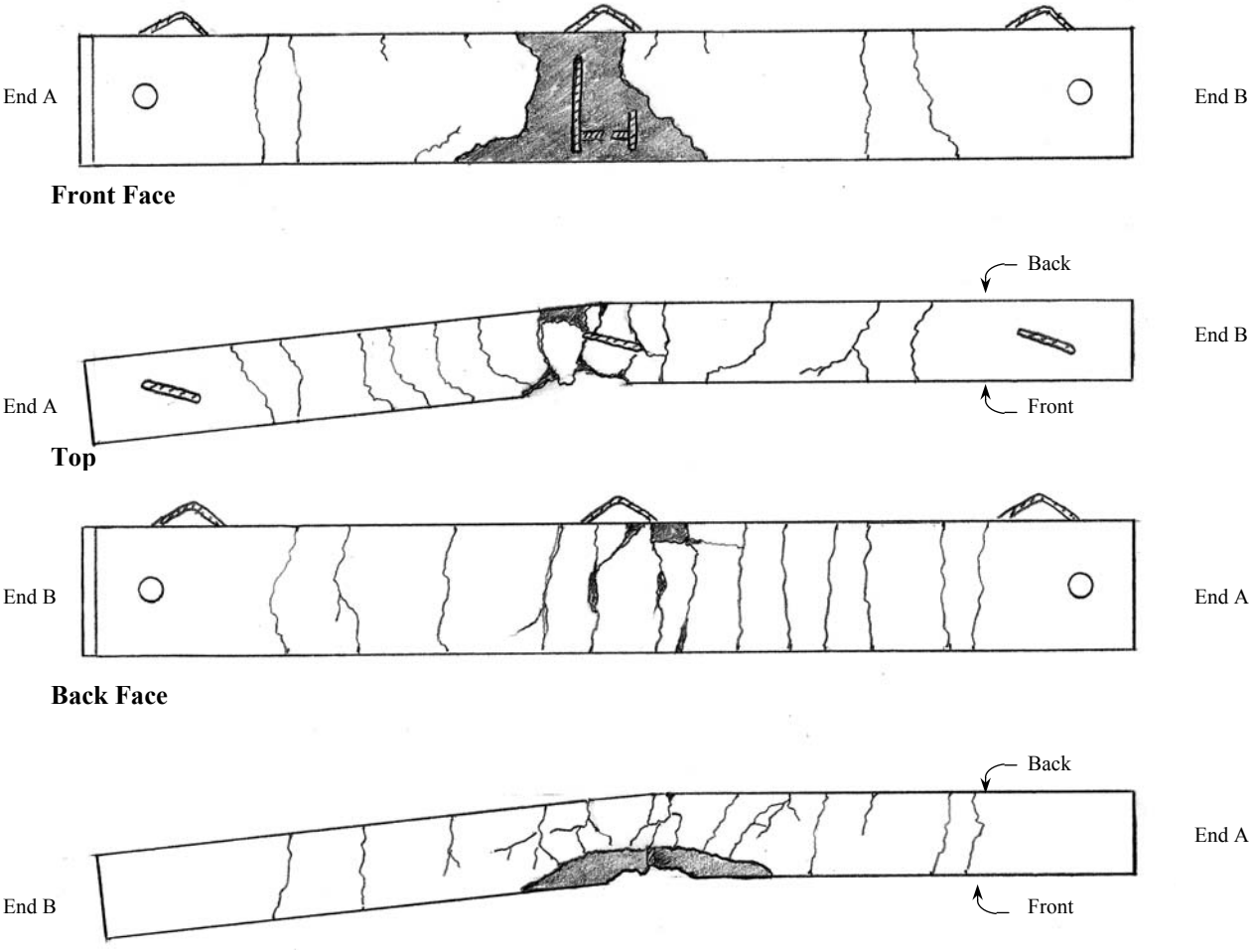

Figure B.1 – Beam 1A blast damage

Beam Designation: 1B

Explosives Used: 10 lbs (4.54 kg) of C-4 **Face-to-Face Spacing of Beams:** 10 ft (3 m)

Description of Damage: The beam experienced extensive cracking and deformation due to the blast load. The reinforcement yielded and approximately 66 in^2 (43000 mm^2) of the front surface was crushed and removed by the blast. The crushed surface revealed the lower half of stirrup No. 12. A short length of the tensile reinforcement between the stirrups is exposed on the front face on both sides of the No. 12 stirrup. The beam experienced through cracking in the middle 1/3 of the beam. Shear cracks are seen approximately 2 ft (0.6 m) from each end. No cracks were found on the front face outside of the crushed concrete area.

Deformation: 3 in (76 mm) **Crater Size in Soil:** 2 ft (0.6 m)

Beam Sketch:

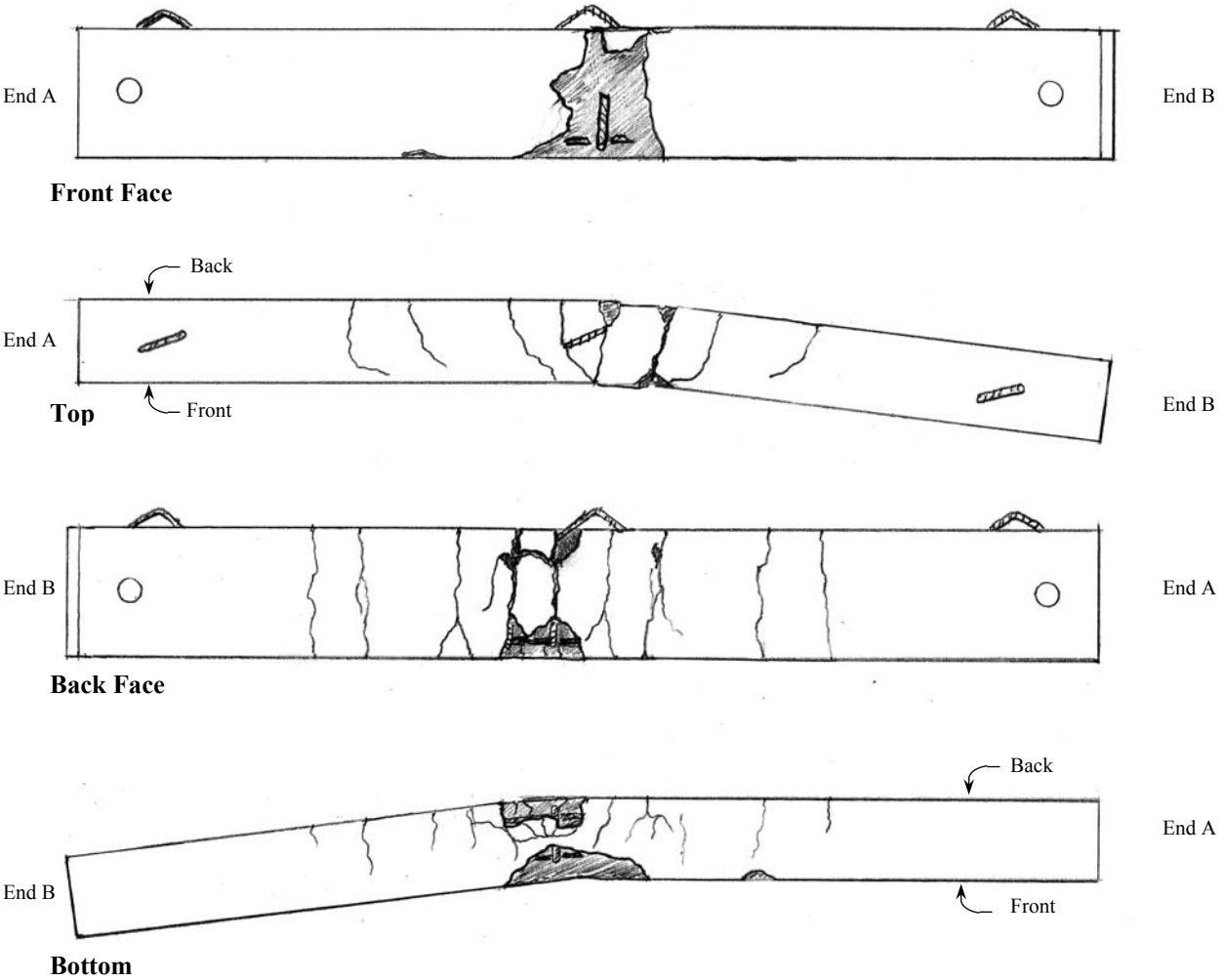

Figure B.2 – Beam 1B blast damage

Beam Designation: 2A

Explosives Used: 11.25 lbs (5.10 kg) of C-4 **Face-to-Face Spacing of Beams:** 10 ft (3 m)

Description of Damage: The beam experienced extensive cracking and deformation due to the blast load. The reinforcement yielded and approximately 77 in^2 (50000 mm^2) of the front surface was crushed and removed by the blast. The crushed surface revealed the lower 1/3 of stirrup No. 11. The beam experienced through cracking along nearly the entire length of the beam. Most of the cracks appear to be flexure cracks with a few shear cracks approximately 2 ft (0.6 m) from each end. The cracks nearest each end were flexure cracks.

Deformation: 1.5 in. (38 mm) **Crater Size in Soil:** 3 ft (1 m)

Beam Sketch:

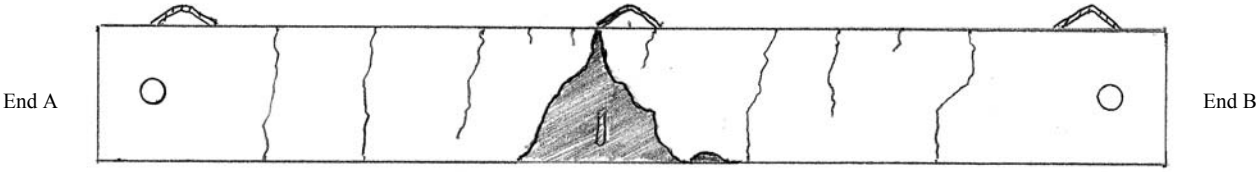

Front Face

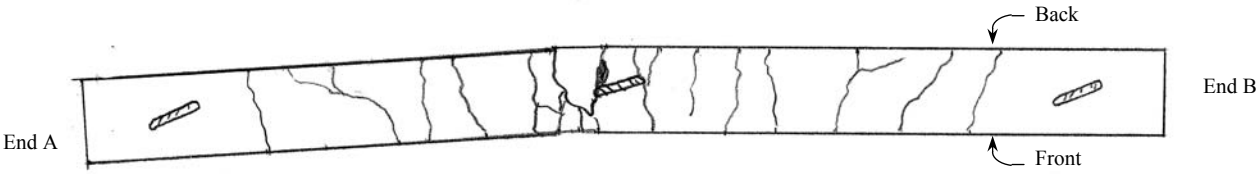

Top

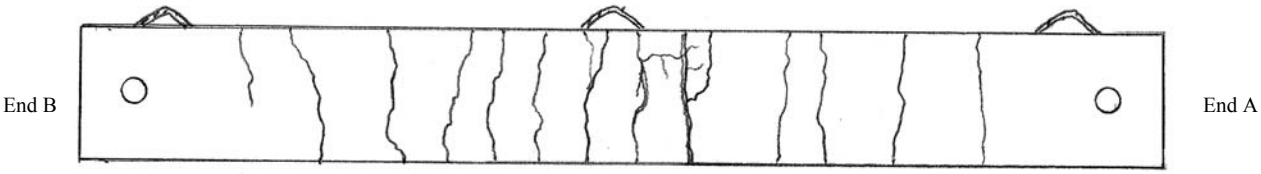

Back Face

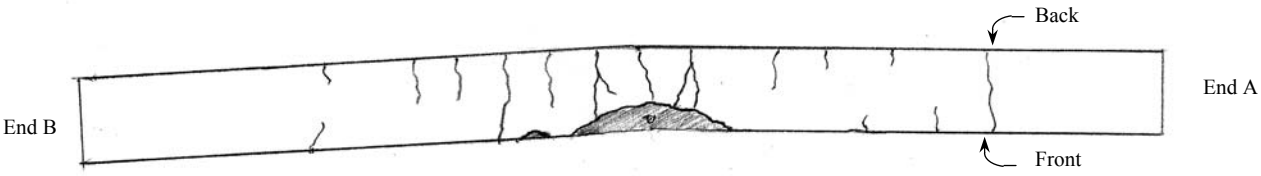

Bottom

Figure B.3 – Beam 2A blast damage

Beam Designation: 2B

Explosives Used: 11.25 lbs (5.10 kg) of C-4 **Face-to-Face Spacing of Beams:** 10 ft (3 m)

Description of Damage: The beam experienced extensive cracking and deformation due to the blast load. The reinforcement yielded and approximately 53 in^2 (34000 mm^2) of the front surface was crushed and removed by the blast. The crushed surface revealed the lower 1/3 of stirrup No. 11. The beam experienced through cracking along nearly the entire length of the beam. Most of the cracks appear to be flexure cracks with several shear cracks approximately two feet from each end. The crack closest to End A appears to be a through flexure crack and the crack closest to End B is also a flexure crack but does not appear to have fully penetrated through the beam.

Deformation: 1.5 in. (38 mm) **Crater Size in Soil:** 3 ft (1 m)

Beam Sketch:

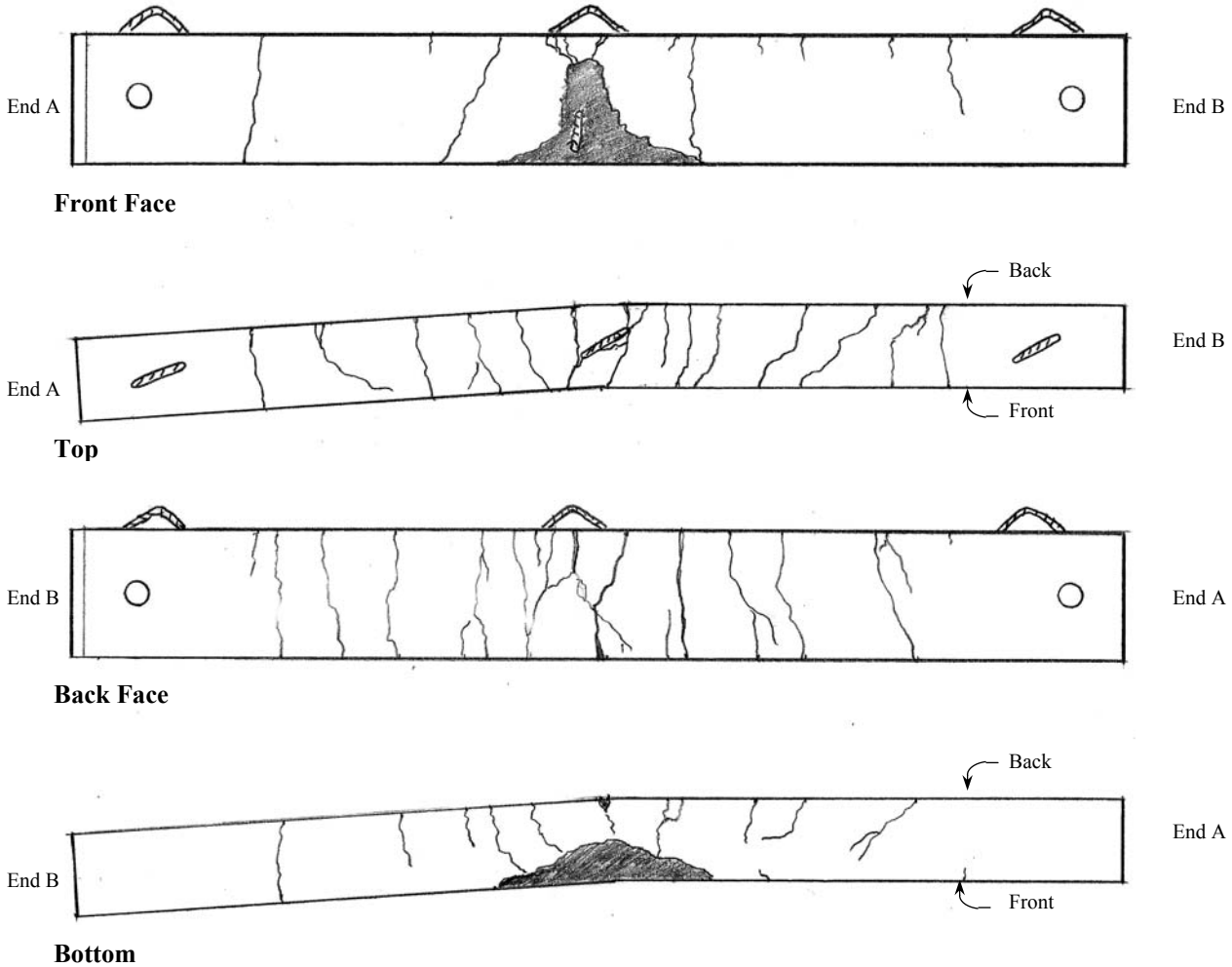

Figure B.4 – Beam 2B blast damage

Beam Designation: 3A

Explosives Used: 15 lbs (6.80 kg) of C-4 **Face-to-Face Spacing of Beams:** 10 ft (3 m)

Description of Damage: This beam experienced the most extensive damage of the eight beams in the study. The beam experienced extensive cracking, deformation, and loss of concrete due to the blast load. The reinforcement yielded and approximately 120 in^2 (77400 mm^2) of the front surface was crushed and removed by the blast. The blast removed most of the concrete around the outside of stirrups No. 13 and 14. The remaining concrete contained within the stirrups appears to have extensive cracking. The crushed surface revealed the lower 1/4 of stirrup No. 12 on the front face. Nearly all of stirrup No. 13 and a large portion of stirrup No. 14 were exposed on all four sides of the beam. The beam experienced through cracking along nearly the entire length of the beam. Most of the cracks appear to be flexure cracks with a several shear cracks at approximately 2 ft (0.6 m) from each end. The cracking on the front and back face appears to line up with the approximate location of stirrups that are located about 1 in. (25 mm) below the surface.

Deformation: 2.5 in. (64 mm) **Crater Size in Soil:** 2½ ft (0.75 m)

Beam Sketch:

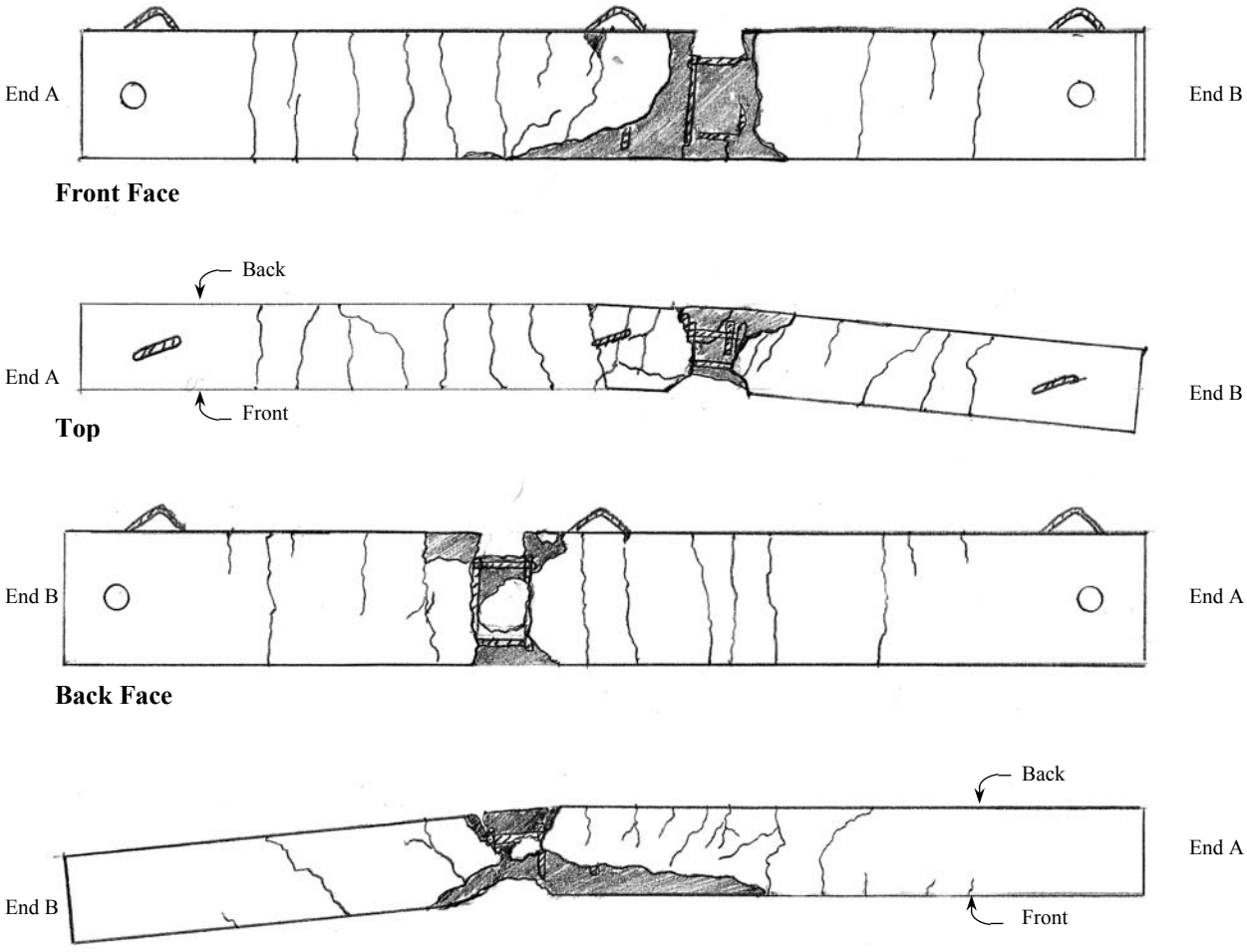

Figure B.5 – Beam 3A blast damage

Beam Designation: 3B

Explosives Used: 15 lbs (6.80 kg) of C-4 **Face-to-Face Spacing of Beams:** 10 ft (3 m)

Description of Damage: The beam experienced extensive cracking, deformation and loss of concrete due to the blast load. The reinforcement yielded and approximately 96 in^2 (62000 mm^2) of the front surface was crushed and removed by the blast. The blast removed most of the concrete around the outside of stirrup No. 11. The remaining concrete contained within the stirrup appears to have extensive cracking. The crushed surface on the front face revealed the lower 2/3 of stirrup No. 11 and approximately 1½ in. (38 mm) of longitudinal reinforcement. Nearly all of stirrup No. 13 and a large portion of stirrup No. 14 were exposed on all four sides of the beam. The beam experienced through cracking along nearly the entire length of the beam. Most of the cracks appear to be flexure cracks with a several shear cracks at approximately two feet from each end. The cracking on the front and back face appears to line up with the approximate location of stirrups located about 1 in. below the surface.

Deformation: 3 in. (76 mm) **Crater Size in Soil:** 2½ ft (0.75 m)

Beam Sketch:

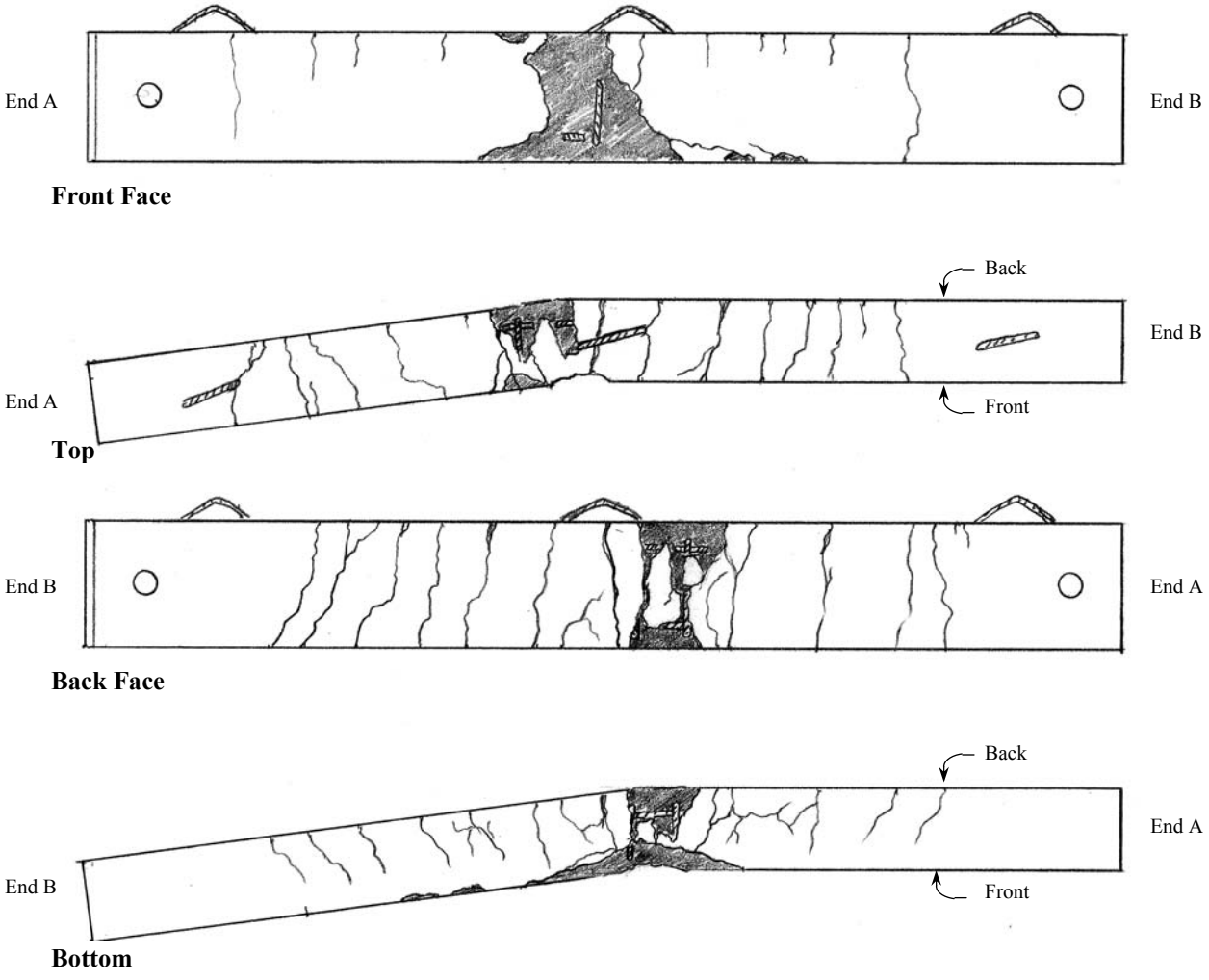

Figure B.6 – Beam 3B blast damage

Beam Designation: 4A

Explosives Used: 6.25 lbs (2.83 kg) of C-4 **Face-to-Face Spacing of Beams:** 10 ft (3 m)

Description of Damage: Beam 4A exhibited no signs of steel yielding and had no permanent horizontal deflection. It had at least 2 through cracks located approximately 4 and 13 in. (100 and 330 mm) to the left of center on the front face of the beam. Five additional cracks go completely through the beam. However, they do not extend all the way to the bottom of the front face. The cracks are all flexural cracks with no evidence of shear cracking. There was no spalling of the concrete on the front surface and all of the concrete appears sound.

Deformation: 0 in. **Crater Size in Soil:** 1 ft (0.3 m)

Beam Sketch:

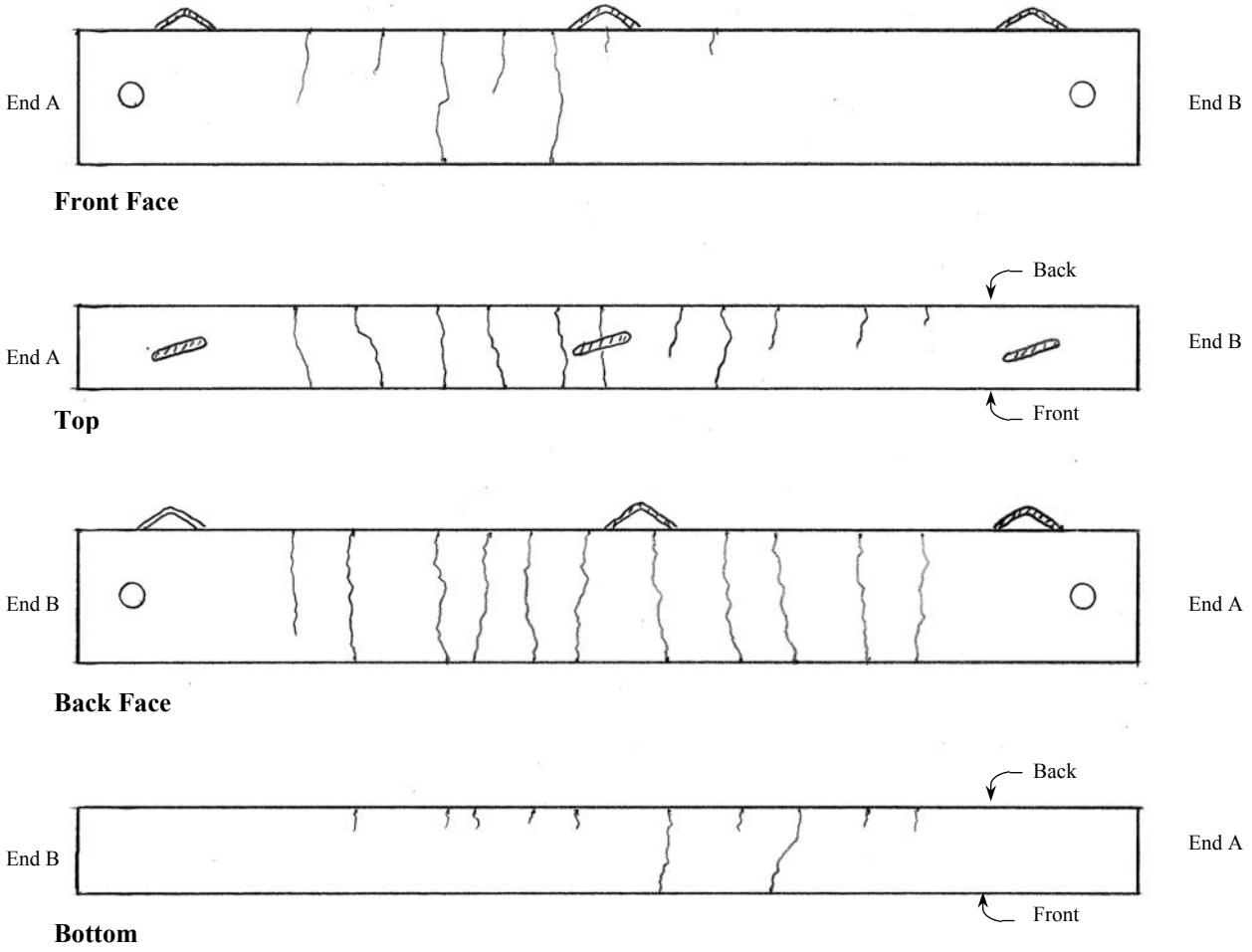

Figure B.7 – Beam 4A blast damage

Beam Designation: 4B

Explosives Used: 6.25 lbs (2.83 kg) of C-4 **Face-to-Face Spacing of Beams:** 10 ft (3 m)

Description of Damage: Beam 4B exhibited no signs of steel yielding and had no permanent horizontal deflection. It had at least 2 complete through cracks located approximately 1 and 11 in. (25 and 280 mm) to the right of center on the front face of the beam. The crack located approximately 21 in. (530 mm) to the right of center on the front face extends the full height of the front face but does not appear to extend all the way though the beam onto the lower half of the back face. The crack 8 in. (200 mm) to the left of center on the front face is just a few inches short of completely cracking the entire way through the beam section. The cracks are all flexural cracks with the exception of a shear crack on the top of the beam 13 in. (330 mm) to the right of center. There was no spalling of the concrete on the front surface and all of the concrete appears sound.

Deformation: 0 in. **Crater Size in Soil:** 1 ft (0.3 m)

Beam Sketch:

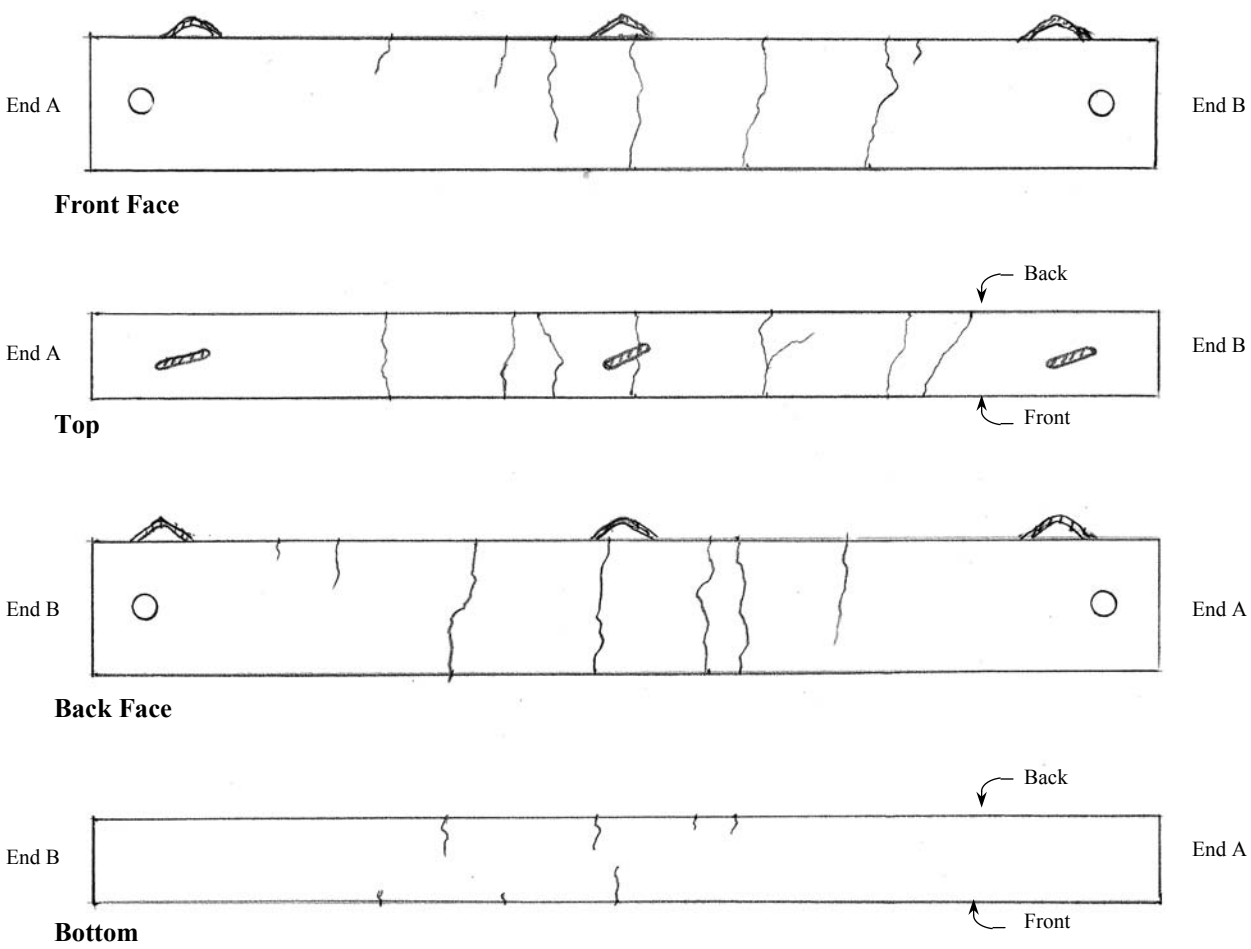

Figure B.8 – Beam 4B blast damage

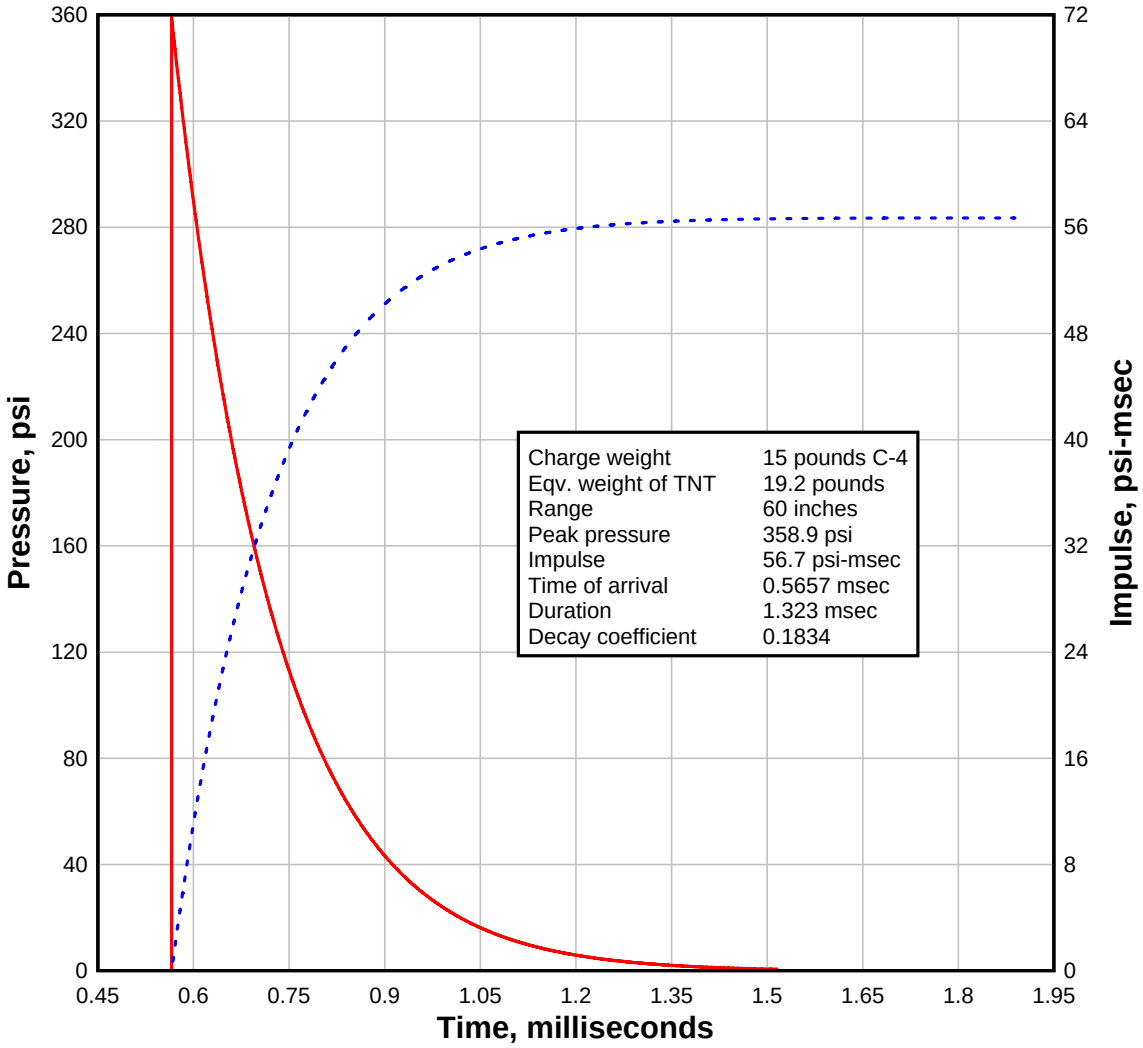

Figure C-3: Anticipated incident pressure history for Set 3 with charge weight of 15 lbs (6.80 kg) (ConWep 2.1.0.3).

1 psi = 0.006895 MPa

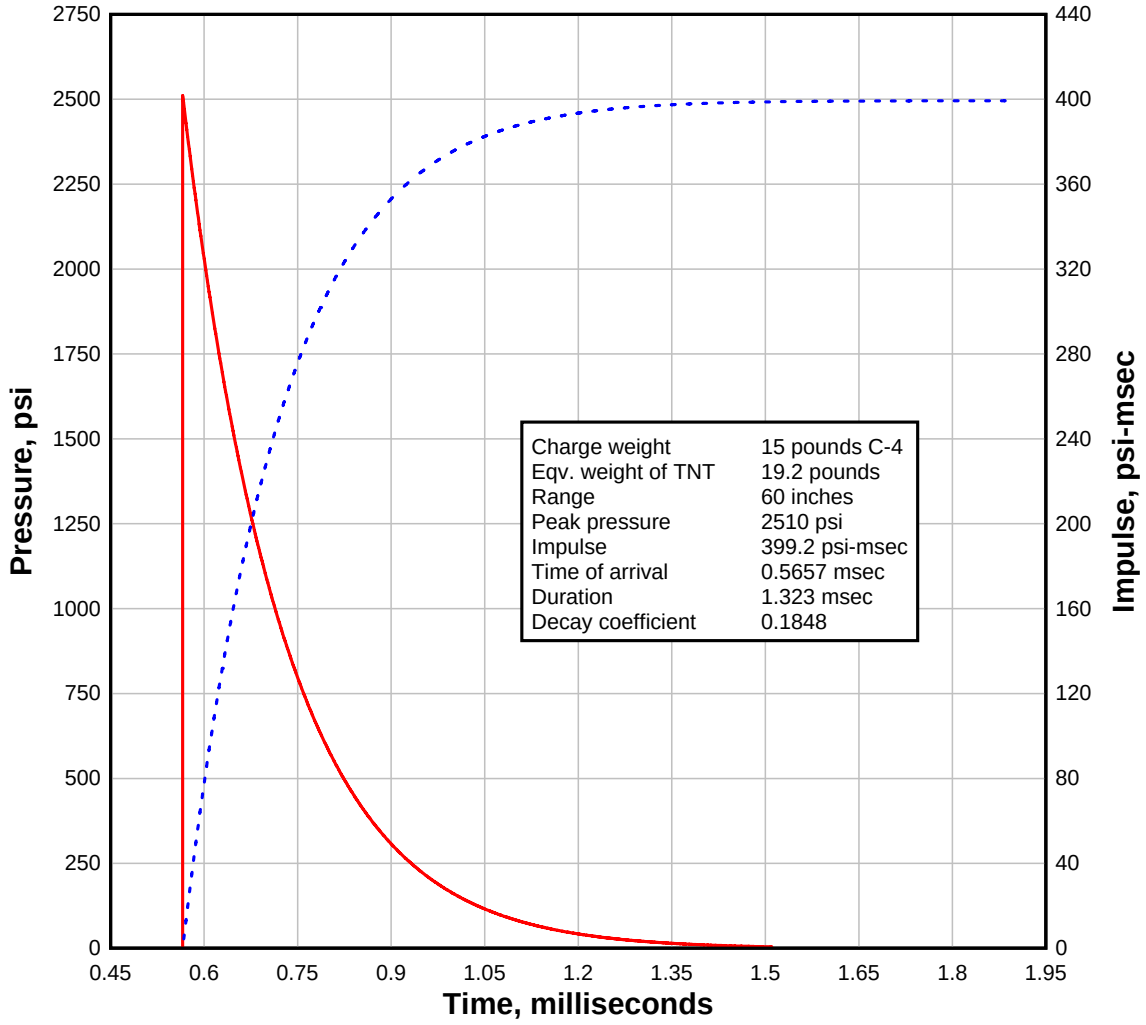

Figure C-4: Anticipated reflected pressure history for Set 3 with charge weight of 15 lbs (6.80 kg) (ConWep 2.1.0.3).

1 psi = 0.006895 MPa

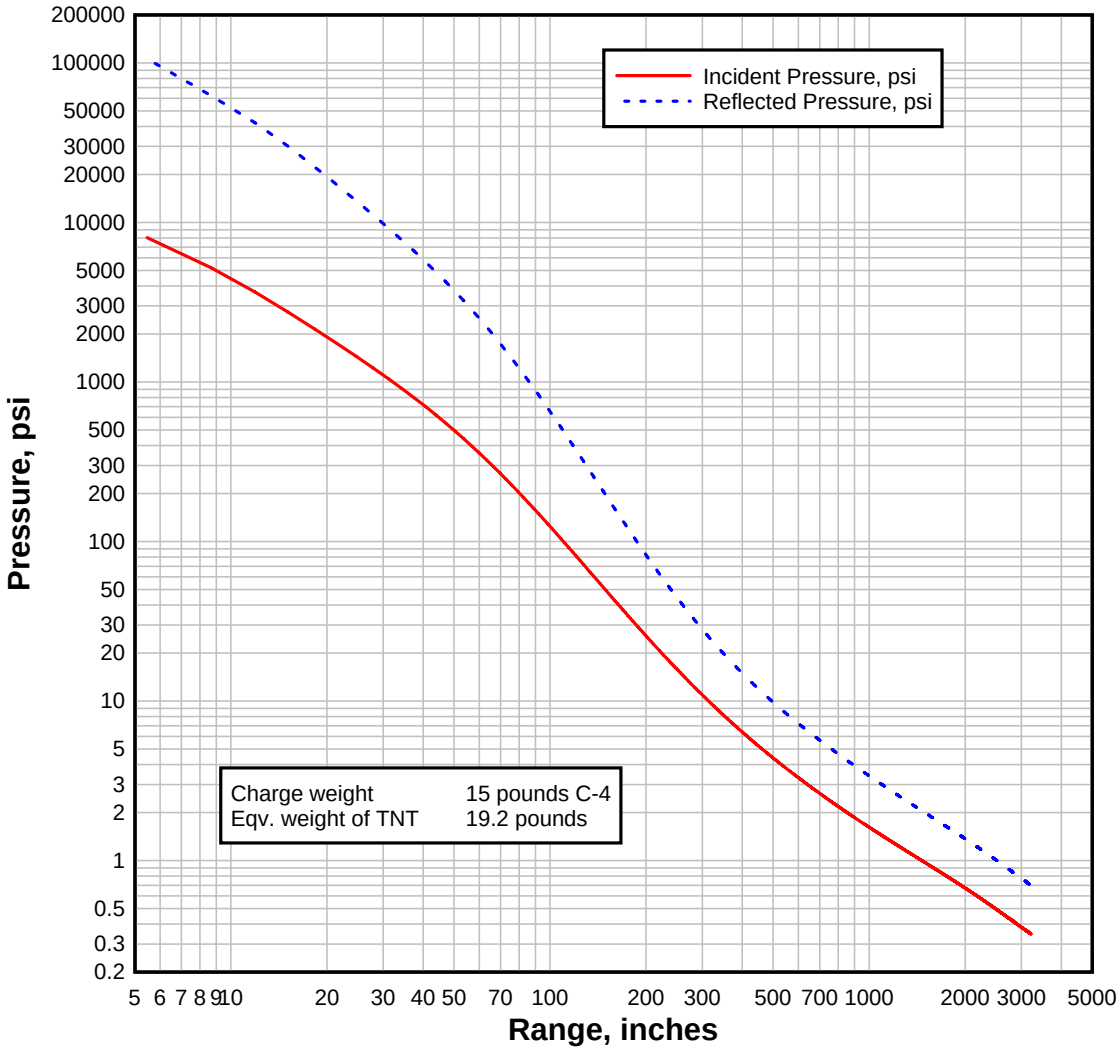

Figure C-5: Anticipated incident and reflected pressure vs. range for charge weight of 15 lbs (6.80 kg). Note how quickly the incident pressure dissipates, reaching approximately 1 psi (6895 Pa) at 125 ft (38 m) from point of detonation (ConWep 2.1.0.3).

1 psi = 0.006895 MPa
1 in = 25.4 mm

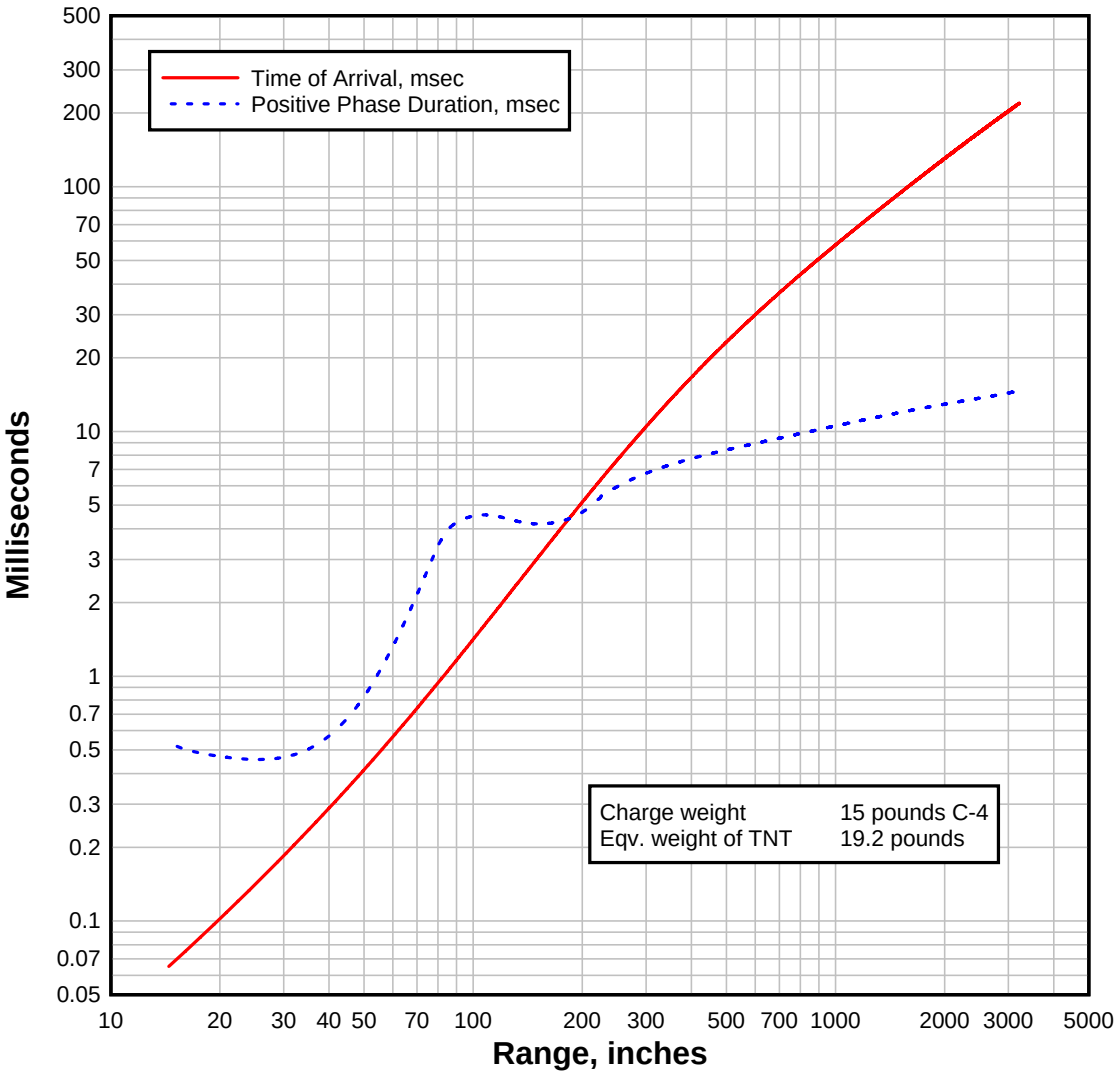

Figure C-6: Anticipated time of arrival and duration vs. range for charge weight of 15 lbs (6.80 kg). Note that it takes about 0.6 msec for the incident to reach the face of the beams 60 in. (1.5 m) from the point of detonation. Additionally, the duration of the incident pressure on the beams is less than 1.5 msec (ConWep 2.1.0.3).

1 in = 25.4 mm

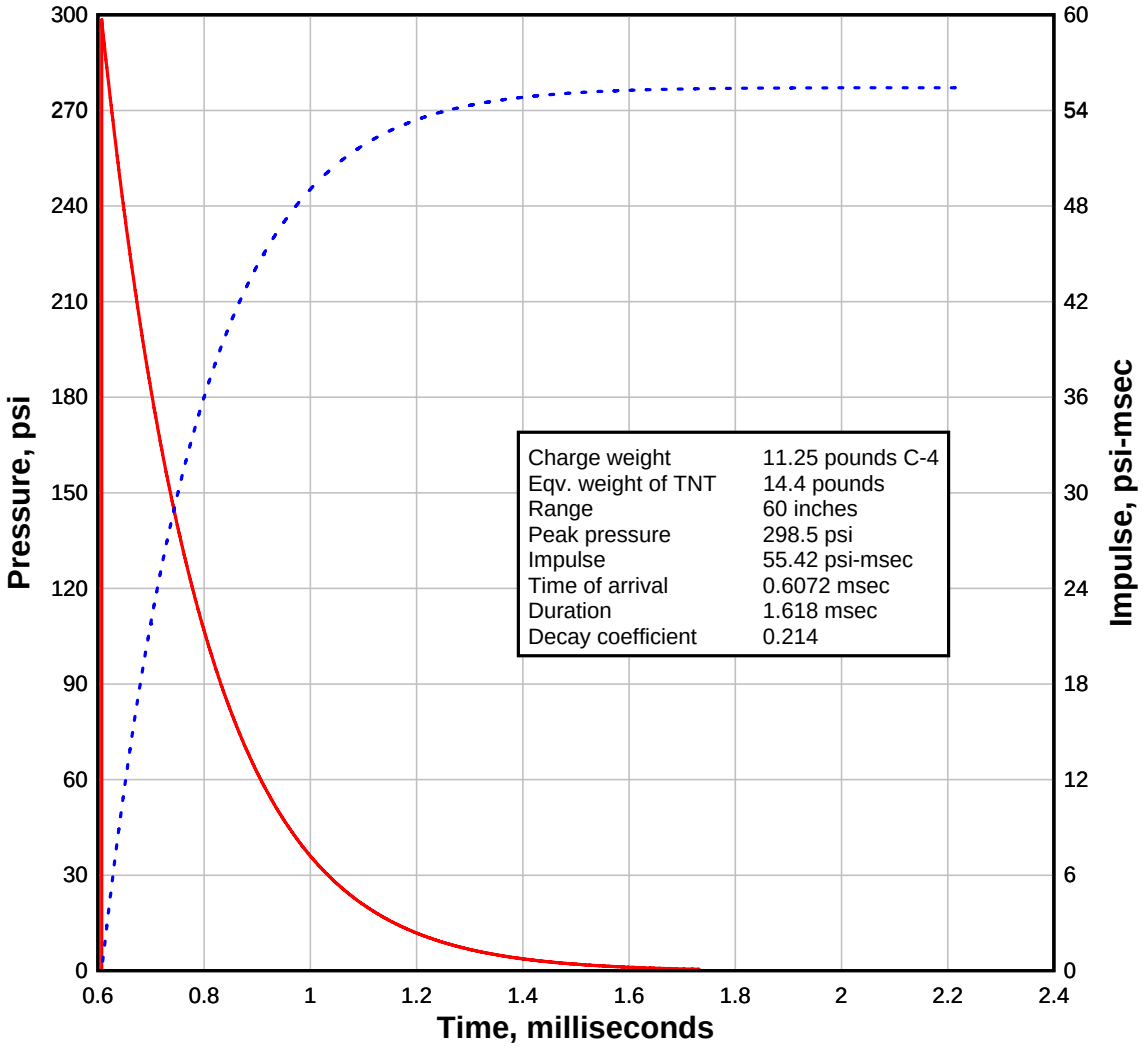

Figure C-7: Anticipated incident pressure history for Set 2 with charge weight of 11.25 lbs (5.10 kg) (ConWep 2.1.0.3).

1 psi = 0.006895 MPa

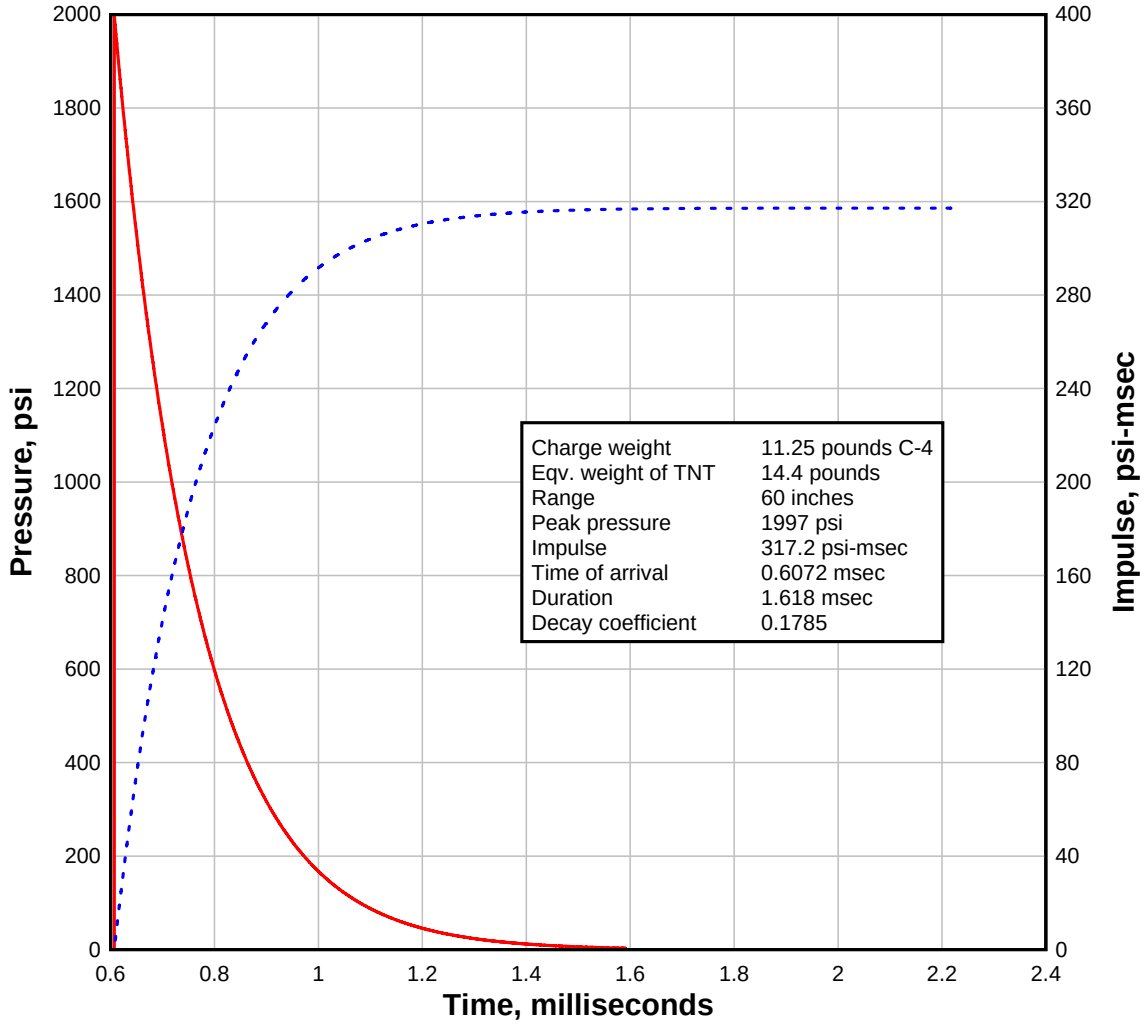

Figure C-8: Anticipated reflected pressure history for Set 2 with charge weight of 11.25 lbs (5.10 kg) (ConWep 2.1.0.3).

1 psi = 0.006895 MPa

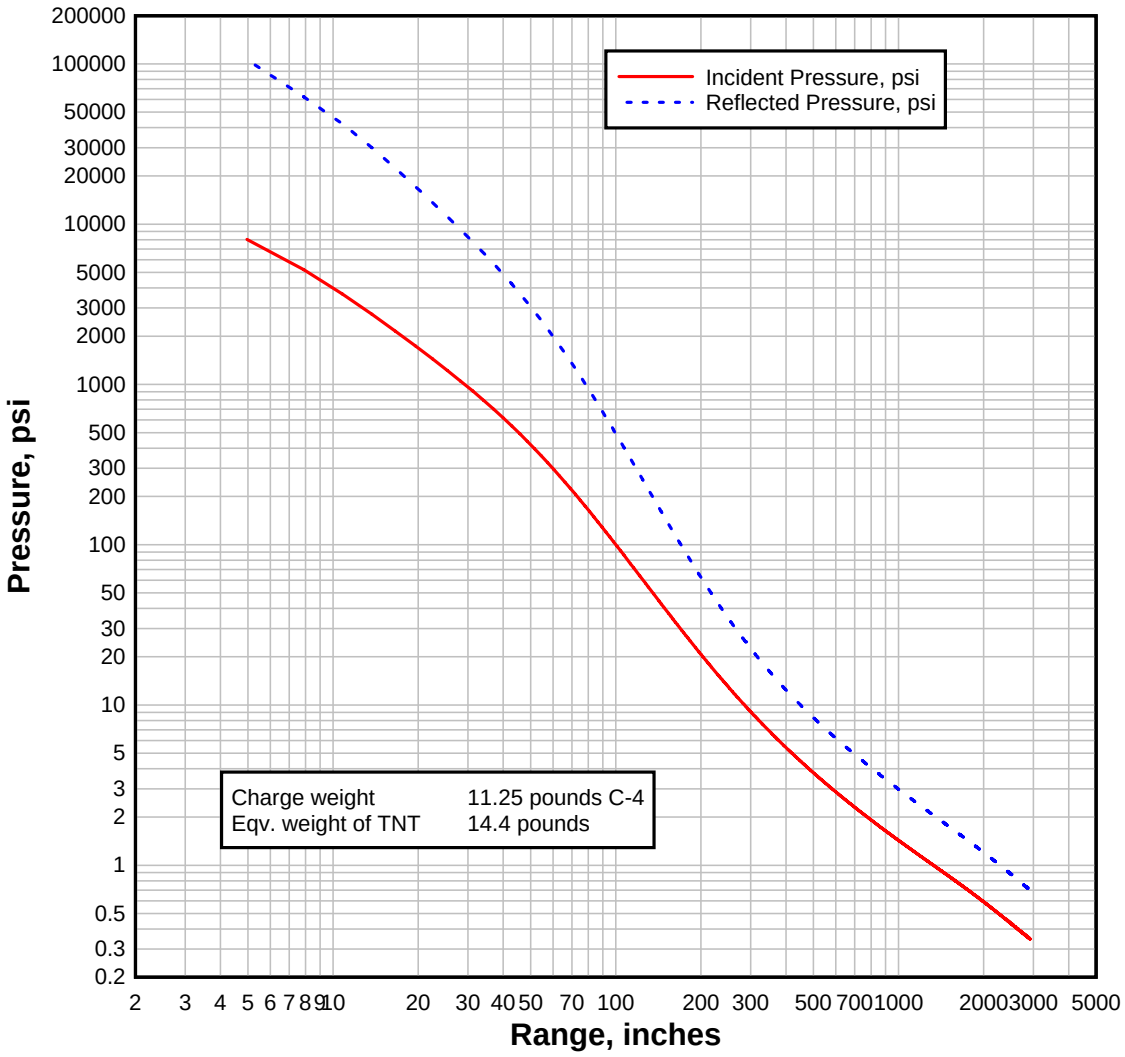

Figure C-9: Anticipated incident and reflected pressure vs. range for charge weight of 11.25 lbs (5.10 kg). Note how quickly the incident pressure dissipates, reaching approximately 1 psi (6895 Pa) at 100 ft (30.5 m) from point of detonation (ConWep 2.1.0.3).

1 psi = 0.006895 MPa
1 in = 25.4 mm

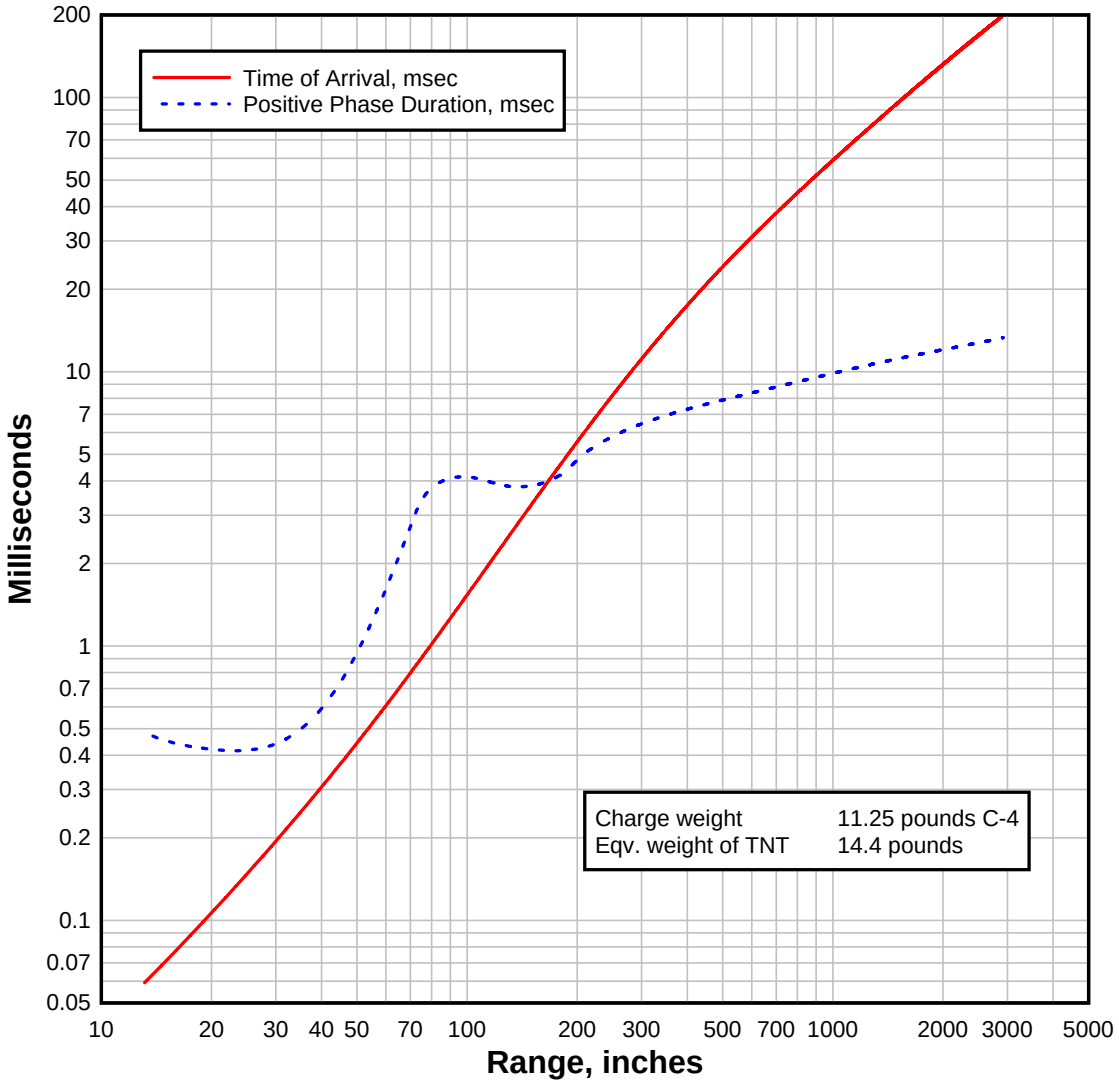

Figure C-10: Anticipated time of arrival and duration vs. range for charge weight of 11.25 lbs (5.10 kg). Note that it takes about 0.6 msec for the incident to reach the face of the beams 60 in. (1.5 m) from the point of detonation. Additionally, the duration of the incident pressure on the beams is less than 1.7 msec (ConWep 2.1.0.3).

1 in = 25.4 mm

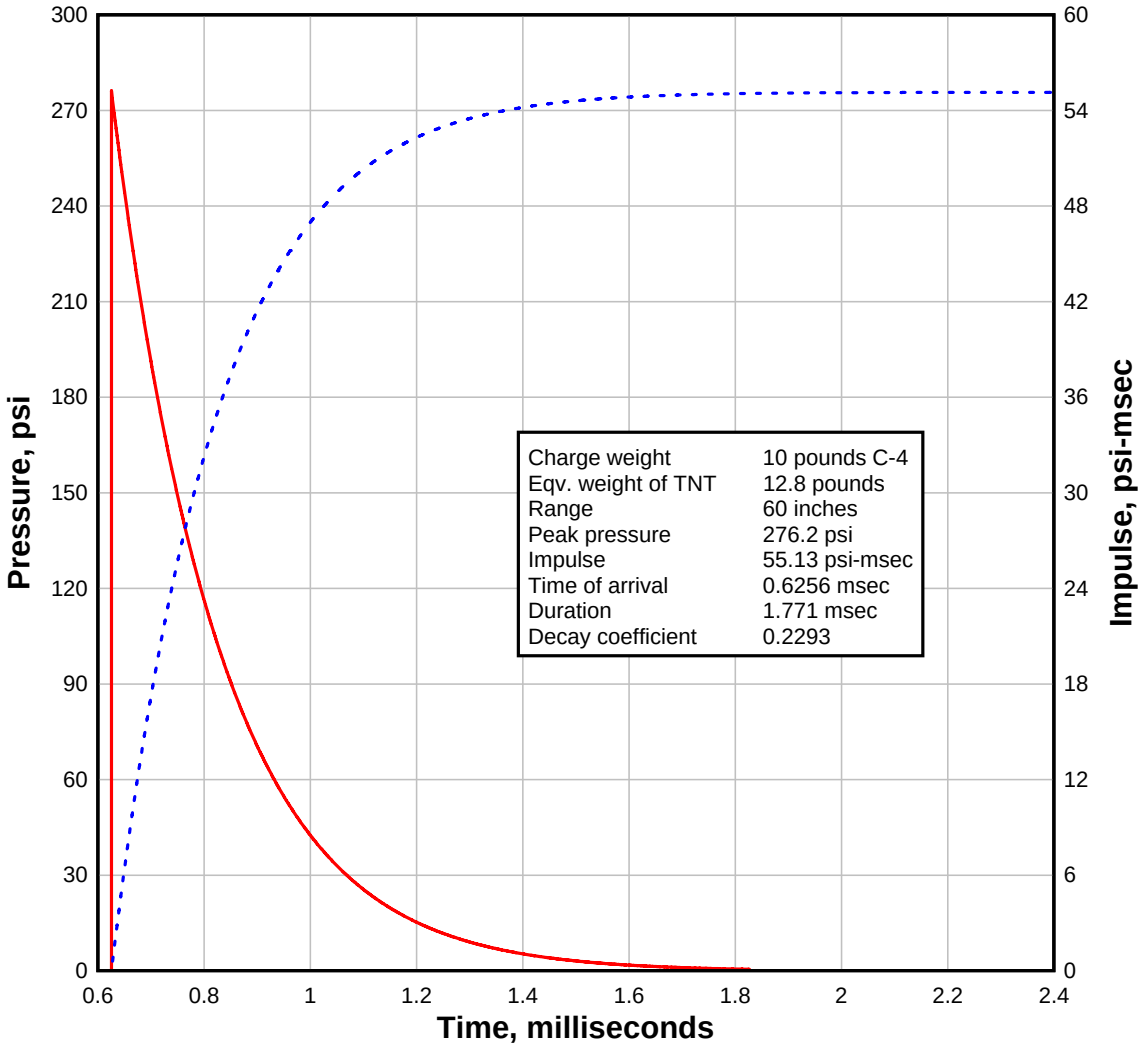

Figure C-11: Anticipated incident pressure history for Set 1 with charge weight of 10 lbs (4.54 kg) (ConWep 2.1.0.3).

1 psi = 0.006895 MPa

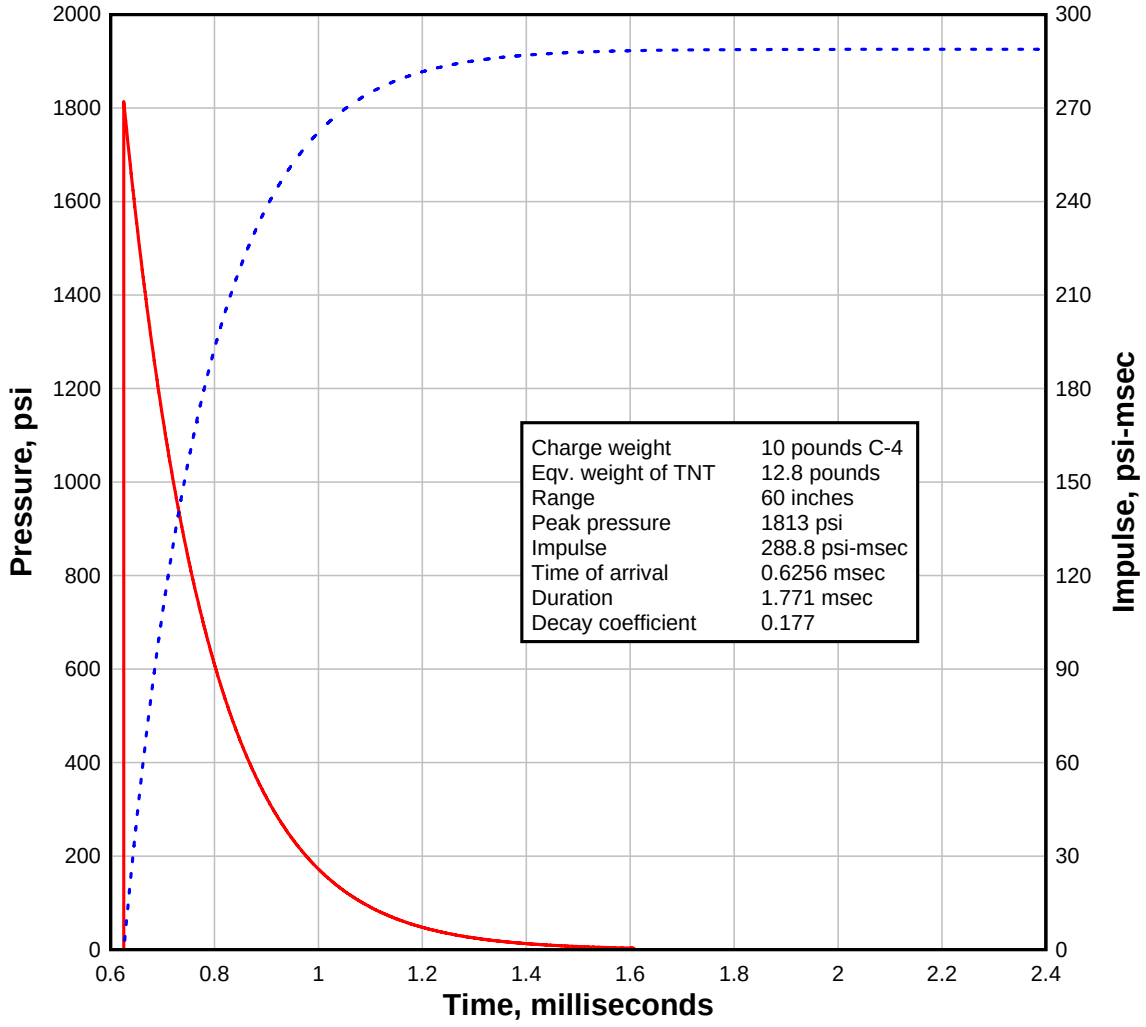

Figure C-12: Anticipated reflected pressure history for Set 1 with charge weight of 10 lbs (4.54 kg) (ConWep 2.1.0.3).

1 psi = 0.006895 MPa

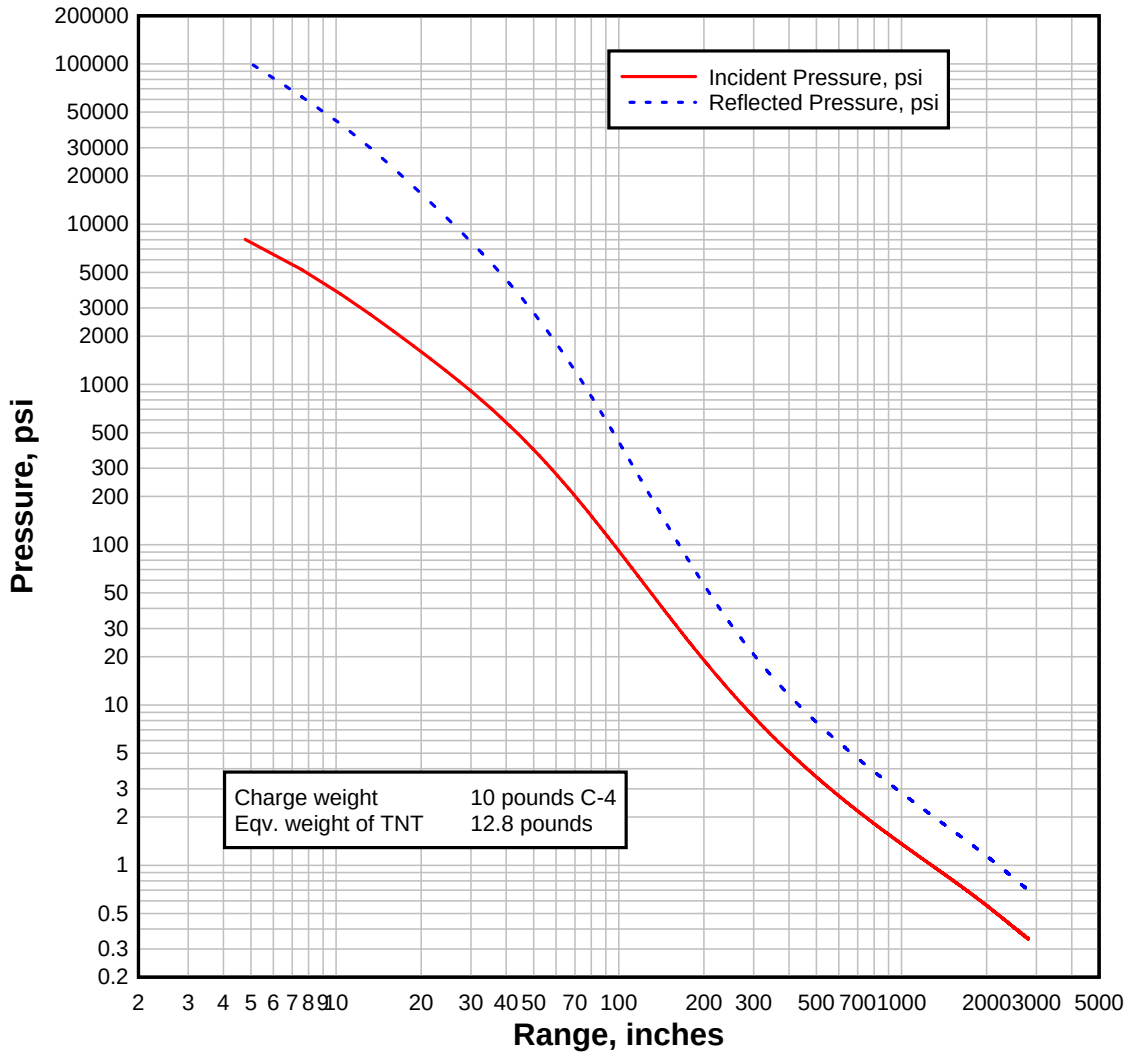

Figure C-13: Anticipated incident and reflected pressure vs. range for charge weight of 10 lbs (4.54 kg). Note how quickly the incident pressure dissipates, reaching approximately 1 psi (6895 Pa) at 95 ft (29 m) from point of detonation (ConWep 2.1.0.3).

1 psi = 0.006895 MPa
1 in = 25.4 mm

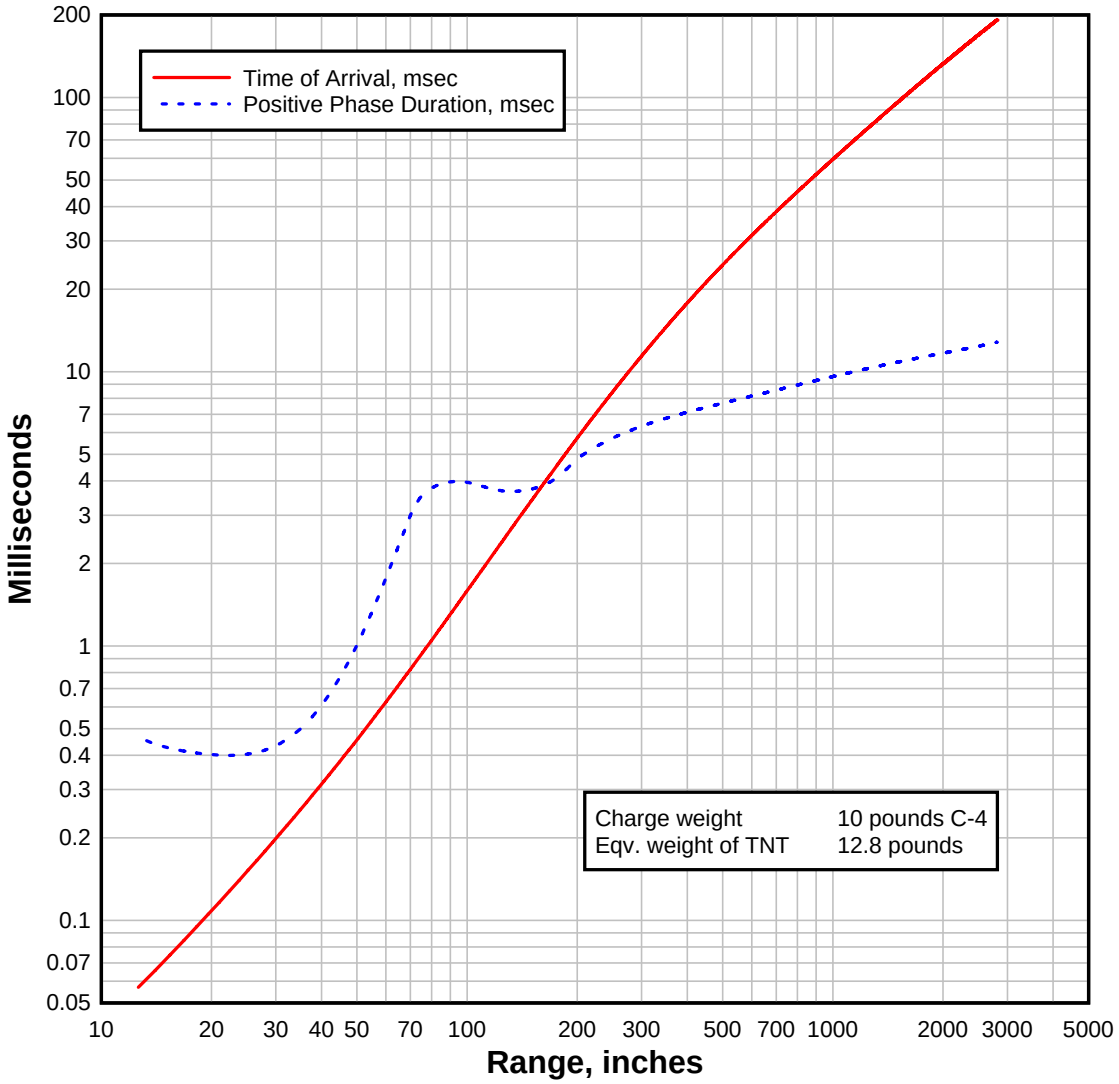

Figure C-14: Anticipated time of arrival and duration vs. range for charge weight of 10 lbs (4.54 kg). Note that it takes just over 0.6 msec for the incident to reach the face of the beams 60 in. (1.5 m) from the point of detonation. Additionally, the duration of the incident pressure on the beams is about 2 msec (ConWep 2.1.0.3).

1 in = 25.4 mm

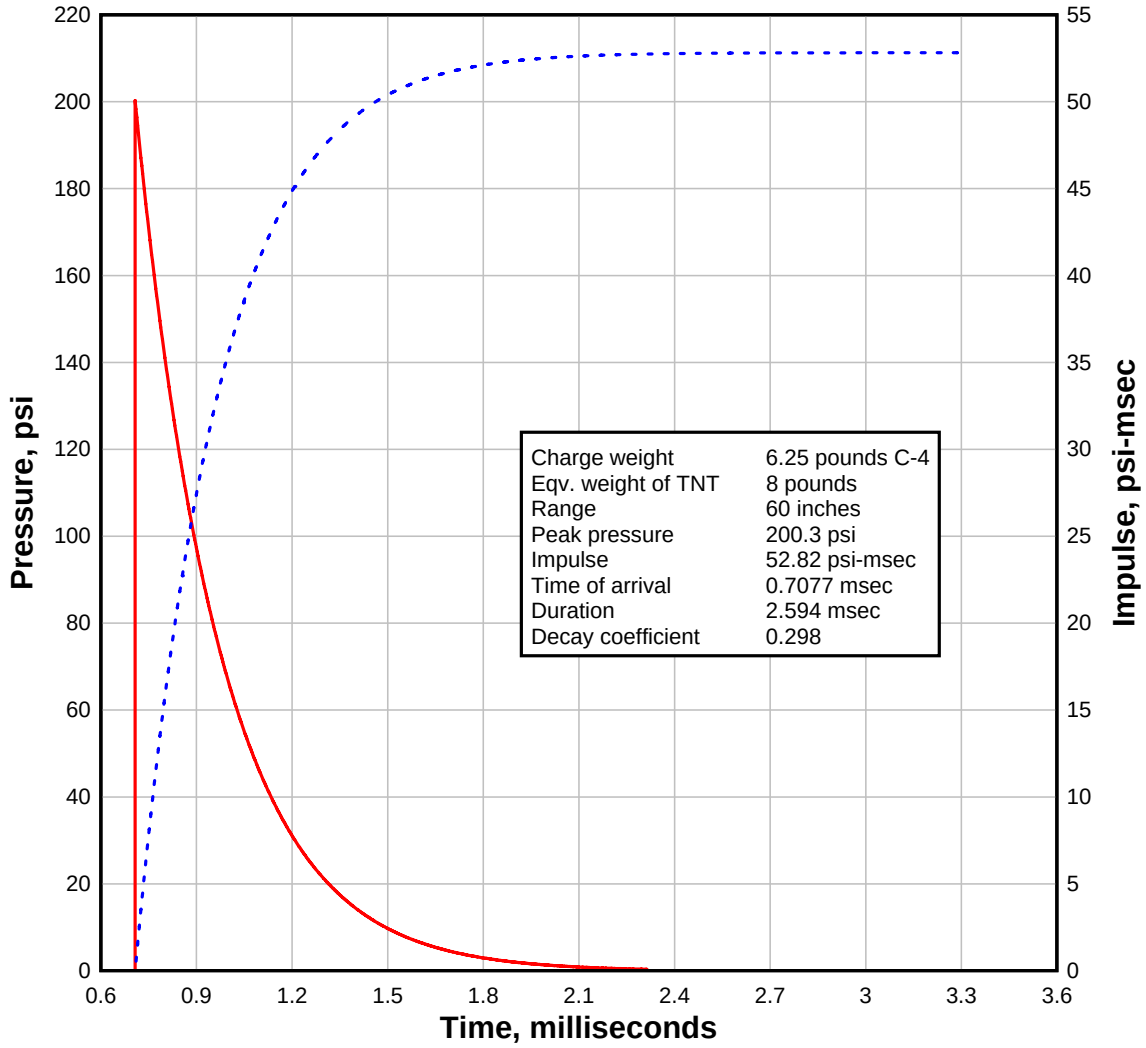

Figure C-15: Anticipated incident pressure history for Set 4 with charge weight of 6.25 lbs (2.83 kg) (ConWep 2.1.0.3).

1 psi = 0.006895 MPa

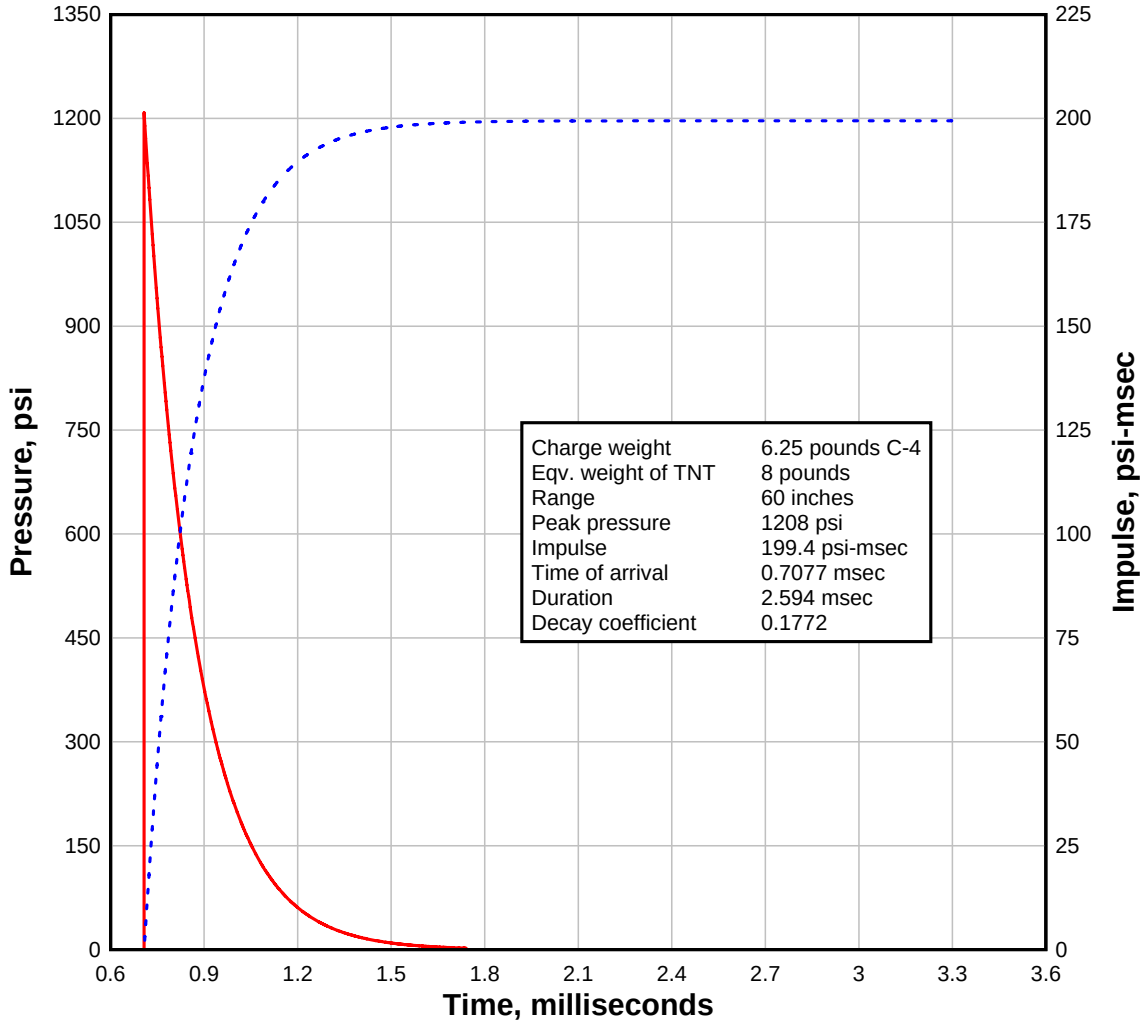

Figure C-16: Anticipated reflected pressure history for Set 4 with charge weight of 6.25 lbs (2.83 kg) (ConWep 2.1.0.3).

1 psi = 0.006895 MPa

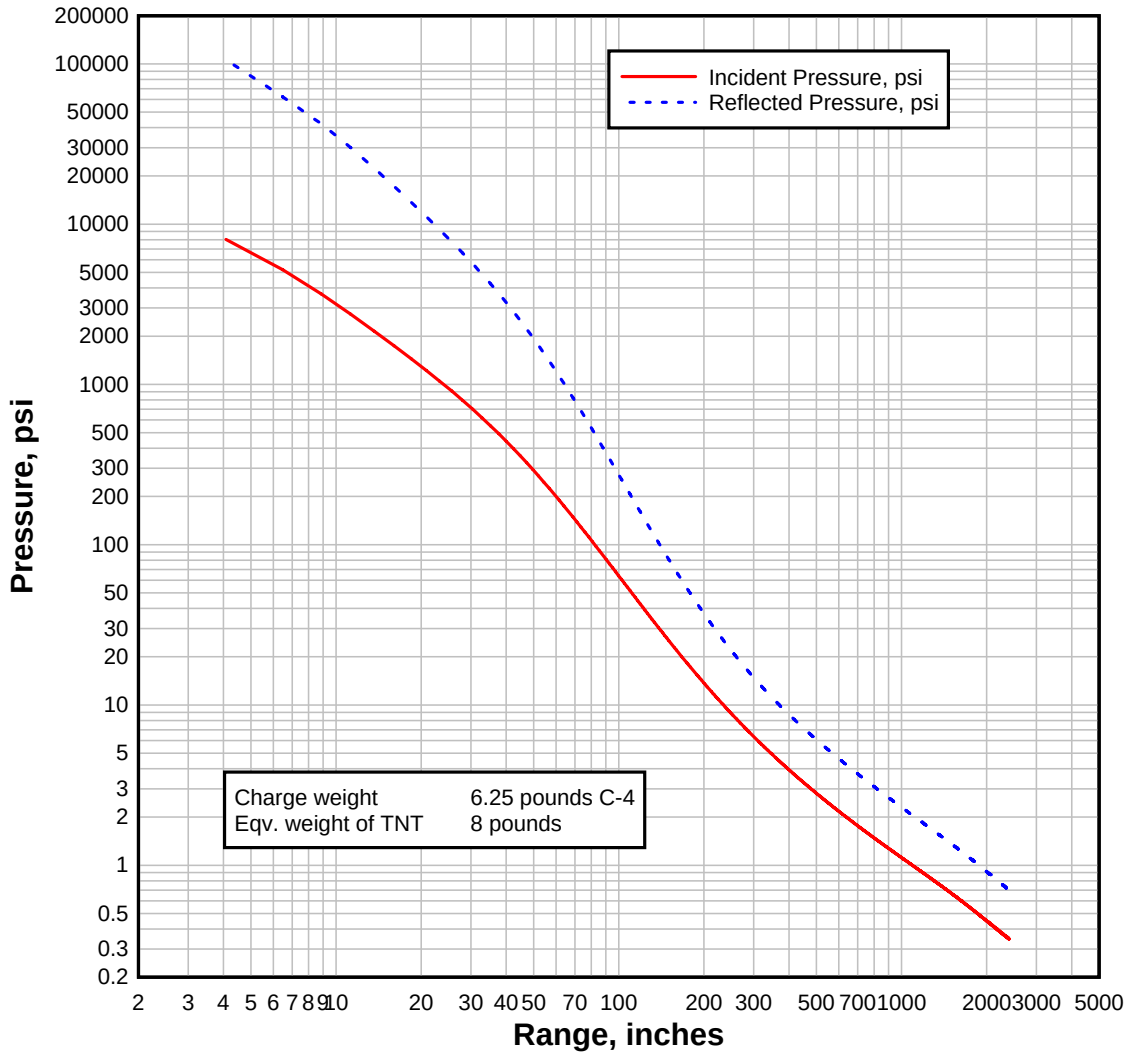

Figure C-17: Anticipated incident and reflected pressure vs. range for charge weight of 6.25 lbs (2.83 kg). Note how quickly the incident pressure dissipates, reaching approximately 1 psi (6895 Pa) at 85 ft (26 m) from point of detonation (ConWep 2.1.0.3).

1 psi = 0.006895 MPa
1 in = 25.4 mm

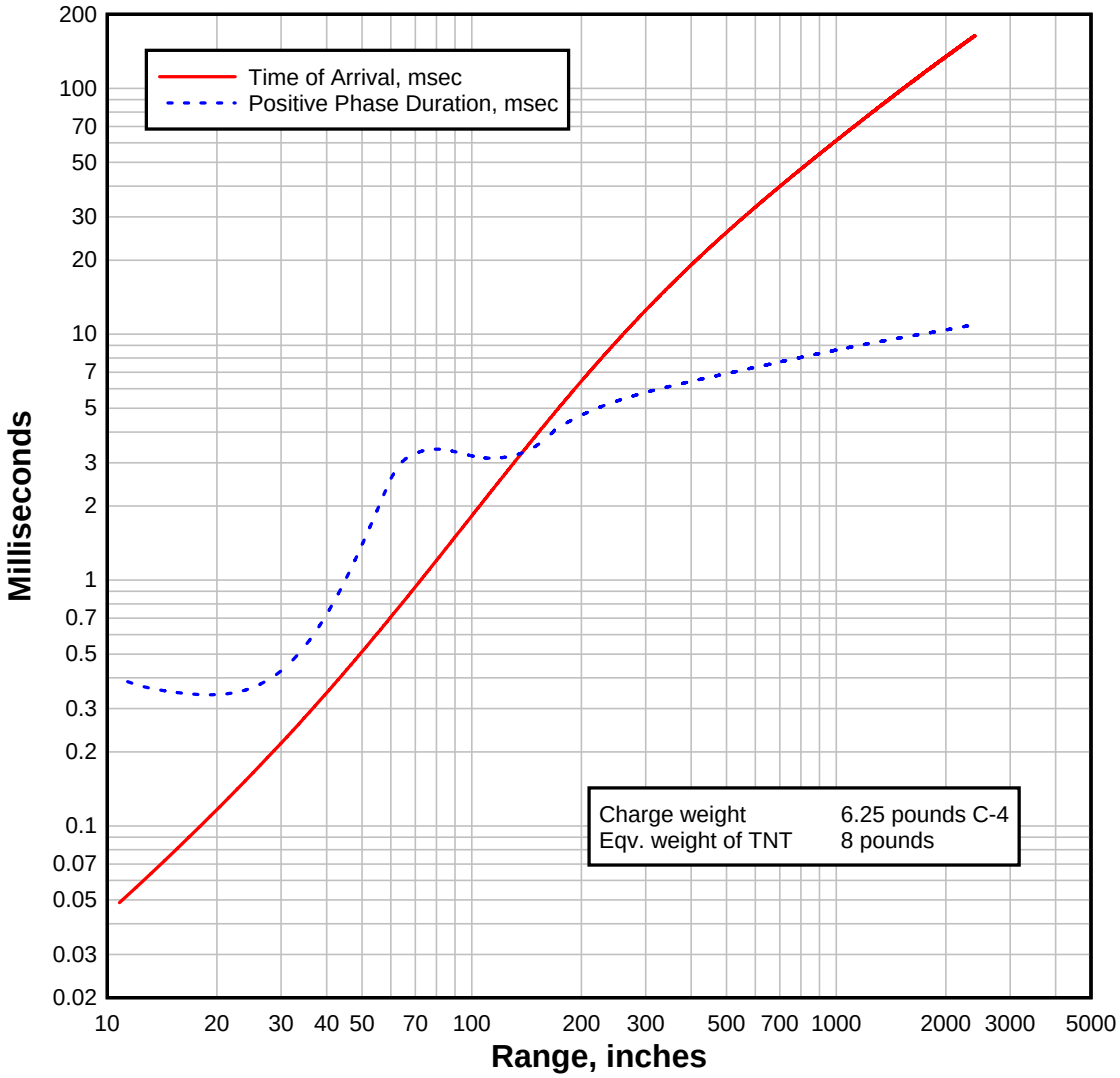

Figure C-18: Anticipated time of arrival and duration vs. range for charge weight of 6.25 lbs (2.83 kg). Note that it takes about 0.7 msec for the incident to reach the face of the beams 60 in. (1.5) from the point of detonation. Additionally, the duration of the incident pressure on the beams is close to 3 msec (ConWep 2.1.0.3).

1 in = 25.4 mm